



Modeling the sensitivity of snowmelt, soil moisture and streamflow generation to climate over the Canadian Prairies using a basin classification approach

Zhihua He¹, Kevin Shook¹, Christopher Spence², John W. Pomeroy¹, and Colin J. Whitfield^{3,4}

¹Centre for Hydrology, University of Saskatchewan, Saskatoon, Saskatchewan, Canada

²Environment and Climate Change Canada, Saskatoon, Saskatchewan, Canada

³School of Environment and Sustainability, University of Saskatchewan, Saskatoon, Saskatchewan, Canada

⁴Global Institute for Water Security, University of Saskatchewan, Saskatoon, Saskatchewan, Canada

Correspondence: Zhihua He (zhh624@mail.usask.ca)

Abstract.

This study evaluated the effects of climate perturbations on snowmelt, soil moisture and streamflow generation in small Canadian Prairie basins using a modeling approach based on classification of basin biophysical and hydraulic parameters. Seven basin classes that encompass the entirety of the Prairie ecozone in Canada were determined by cluster analysis of biophysical characteristics. Individual semi-distributed virtual basin (VB) models representing these classes were parameterized in the Cold Regions Hydrological Model (CRHM) platform which includes modules for snowmelt and sublimation, soil freezing and thawing, actual evapotranspiration (ET), soil moisture dynamics, groundwater recharge and depressional storage dynamics including fill and spill runoff generation and variable connected areas. Precipitation (P) and temperature (T) perturbation scenarios covering the range of climate model predictions for the 21st century were used to evaluate climate sensitivity of hydrological processes in individual land cover and basin types across the Prairie ecozone. Results indicated that snow accumulation in wetlands had a greater sensitivity to P and T than that in croplands and grasslands in all the basin types. Wetland soil moisture was also more sensitive to T than the cropland and grassland soil moisture. Jointly influenced by land cover distribution and local climate, basin-average snow accumulation was more sensitive to T in the drier and grassland-characterized basins than in the wetter basins dominated by cropland, whilst basin-average soil moisture was most sensitive to T and P perturbations in basins typified by pothole depressions and broad river valleys. Annual streamflow had the greatest sensitivities to T and P in the dry and poorly connected Interior Grassland basins but the smallest in the wet and well-connected Southern Manitoba basins. The ability of P to compensate for warming induced reductions in snow accumulation and streamflow was much higher in the wetter and cropland-dominated basins than in the drier and grassland-characterized basins, whilst decreases in cropland soil moisture induced by the maximum expected warming of 6 °C could be fully offset by P increase of 11% in all the basins. These results can be used to 1) identify locations which had the largest hydrological sensitivities to changing climate; and 2) diagnose underlying processes responsible for hydrological responses to expected climate change. Variations of hydrological sensitivity in land cover and basin types suggest that different water management and adaptation methods are needed to address enhanced water stress due to expected climate change in different regions of the Prairie ecozone.



1 Introduction

25 The Canadian Prairies Ecozone occupies 450,000 km² from Alberta in the west to Manitoba in the east (Figure 1). This agricultural region features a semi-arid to sub-humid, cold, continental climate with a long-term mean annual precipitation of less than 500 mm, approximately one-third of which is snowfall (Shahabul Alam and Elshorbagy, 2015). The Prairies in their natural state were extensively covered by grasslands and topographic depressions filled with wetlands. Now they are the most extensive agricultural land base in Canada, whilst providing crucial habitat for waterfowl and other wetland and grassland-associated animals (Anteau et al., 2016; Zhang et al., 2021). Spring snowmelt is the major water source of runoff in the Prairies and the extensive depressions play important roles in storing, evaporating and transporting snow and surface runoff (Pomeroy et al., 2022; Fang and Pomeroy, 2009; Costa et al., 2020; Unduche et al., 2018). Prairie hydrological states can vary widely from drought to deluge (Johnson et al., 2005). Evaluating the sensitivity of Prairie hydrology to climate perturbation would help inform adaptation of water management to future climate changes.

35 The Canadian Prairies are projected to experience relatively rapid climate change in the 21st century. Air temperatures are projected to increase substantively during the next few decades. For example, mean annual temperature is predicted to increase by 1.0 °C to 6.0 °C in most of the Prairies by 2100, compared to 1986–2005 (Bush and Lemmen 2019). Similarly, results from regional climate models (RCMs) indicate that mean annual temperatures in the Prairie Pothole region will increase by 1.8 °C to 4 °C by the end of this century (Withey and van Kooten, 2011). However, projections of future precipitation are much less certain. Johnson et al. (2005) reported that changes in Prairie precipitation in the 21st century could decrease 20% in some areas and increase 20% in others, whilst Bush and Lemmen (2019) predicted that mean annual precipitation will rise by up to 25% in the western Prairie but decrease by –0.2% in the southern Prairie (with differing seasonal responses), compared to 1986–2005. Jiang et al. (2017) projected that seasonal precipitation in Alberta will change from –25% to 36% by the end of 21st century, compared to 1961–1990. Uncertainty in the projected precipitation is attributed to the mismatch between the coarse resolutions of general circulation models (GCMs) or RCMs and the scale of convective precipitation generation in the Prairies (Zhang et al., 2011), which is not always well parameterized in climate models (Zhang et al., 2021). The large uncertainty in climate model projections can restrict their practical application for predicting future hydrology in the Prairies. An alternative method is to add changes to baseline temperature and precipitation conditions informed by ensembles of GCM and RCM projections to represent the range of uncertainty in the projections. This delta method has proven useful to assess hydrological sensitivity to climate perturbations in the Canadian Prairies and nearby regions (Rasouli et al., 2019; Spence et al., 2022a). Particularly, Kienzle et al. (2012) perturbed 30-year baseline precipitation and temperature observations to represent future climate conditions and provide insights into the responses of seasonal streamflow regimes in the Cline River basin, Alberta. MacDonald et al. (2012) used the delta method to shift baseline climate to represent monthly perturbations in precipitation and temperature and showed the sensitivity of snowpack to climate changes in the North Saskatchewan River basin. However, these sensitivity analyses were limited to small basins or portions of the Prairies (Spence et al. 2022a). Comparison of the hydrological sensitivity to climate change across the entire Canadian Prairie region has not yet been rigorously conducted.



Hydrological models can be effective tools for quantifying the hydrological impacts of climate change. However, complex hydrography such as in the Prairie Pothole Region make hydrological modeling in Prairie basins a highly challenging task (Gray, 1970; Fang et al., 2010; Unduche et al., 2018). First, snowmelt and rainfall runoff may not necessarily contribute flow to the basin outlet, as wetlands store surface runoff until their storage capacity is exhausted. As extra runoff only spills and flows to the basin outlet once no storage capacity remains, the uplands only connect to the channel when downstream wetlands are filled (Shaw et al., 2012; Shook et al., 2015). The fill-spill runoff of wetlands and the intermittent surface hydrological connection within Prairie basins specifically is poorly represented in many hydrological models, as those models typically don't simulate physics of depressional storage (Muhammad et al., 2019). Second, blowing snow and frozen soil infiltration strongly affect the generation of snowmelt runoff in spring (Pomeroy et al., 1998). Snow is redistributed directly into prairie depressions from surrounding agricultural fields (Pomeroy et al., 1993; Fang and Pomeroy, 2009). Infiltration of snowmelt into frozen soil is complicated by multiple factors including snowpack accumulation, initial soil moisture, and soil thermal properties (Gray et al., 2001). Physical representation of thermal dynamics of frozen soil in a hydrological model is prerequisite for successful simulation of snowmelt runoff in the Prairies (Pomeroy et al., 2007; Pomeroy et al., 2022). Third, the typical sparse observations of hydro-meteorological data in the Prairies restrict opportunities to calibrate empirical hydrological models using streamflow (St-Jacques et al., 2018). Streamflow records in the Prairie basins are typically intermittent and characterized by long periods of zero flow (Whitfield et al., 2020), with many stream gauge stations operated seasonally. The gauging network is extremely sparse and considered insufficiently gauged for regionalization of runoff (Samuel et al., 2013). Since streamflow is dominated by spring snowmelt runoff, any calibration from streamflow may bias parameters to certain hydrological processes and seasons. Records of streamflow in the Prairies are therefore not necessarily useful for parameter calibration. The complex hydrology of the Prairies highlights the need for physically-based hydrological modeling approaches where parameters for calculation of snow redistribution, snowmelt runoff, soil moisture, depressional storage and streamflow can be estimated based on basin hydrography and biophysical properties.

Building physically-based hydrological models over the entire Prairie ecozone is nonetheless challenging due to dynamic contributing areas caused by geographically isolated wetlands (Pomeroy et al., 2014; Unduche et al., 2018) resulting in poorly defined drainage basins (Pomeroy et al., 2010). A virtual basin (VB) based modeling approach using hydrological response units (HRUs) to represent the typical land cover and hydrographic land types in the Prairies was successfully used to examine the spatial variability of ET over the Prairies (Armstrong et al., 2015). Moreover, VB modeling informed by basin classification (Wolfe et al., 2019) has been successfully applied for assessing streamflow sensitivity to climate perturbation in the western part of the Prairies (Spence et al., 2022a). This study applies this hydrological modeling approach over the entire Canadian Prairies with the aims of: (1) assessing and comparing hydrological sensitivity to climate by evaluating how snow, soil moisture and runoff processes in different land cover types respond; (2) quantifying and comparing the hydrological sensitivity to climate in all the different basin types across the Prairies; and (3) assessing the degree to which precipitation increases can compensate for the hydrological impacts of warming on Prairie hydrological processes.



90 2 Study area and basin classification

The Canadian Prairie region is in the south-central part of western Canada (N 49°–54°, W 90°–115°, Figure 1), extending 0.45 million km² across the Provinces of Alberta, Saskatchewan, and Manitoba. Mean annual precipitation in the Prairies increases from west to east (Johnson and Poiani, 2016; Wolfe et al., 2019), from 300 mm to 610 mm (1970–2000). Mean annual air temperature over the Prairies ranges from 1°C to 6 °C. The long and cold winter results in 30% of annual precipitation falling
95 as snow. Landscapes in the Prairies are, in general, flat, with millions of small wetland depressions embedded within grassland and cropland landscapes. Wolfe et al. (2019) classified approximately 4100 headwater basins of, on average, 100 km² across the Canadian Prairies into seven biophysical basin classes.

Here, a slightly different classification from Wolfe et al. (2019) is used. This one does not include climate variables in the basin classification but features the same seven classes (Figure 1), and is identical to the one described by Spence et al.
100 (2022a). Cropland is the main land use type in all the seven classes, accounting for 40–65%. Pothole Till (PHT) is the largest class by area (120,881 km²), 65% of which is covered by cropland. The other class dominated by cropland (64%) is Pothole Glaciolacustrine (PGL), which spans 77,844 km². The classes of High Elevation Grasslands (HEG), Interior Grasslands (IG) and Sloped Incised (SI) are characterized by high grassland fractions of 37–49%. HEG is the largest grassland-characterized class (79,667 km²). The Major River Valleys (MRV) class (21,149 km²) is characterized by distinct valleys which cover 17%
105 of the class area, and Southern Manitoba (SM) is the class with the fewest wetlands and the most extensive cropland (34,533 km²). Average depression coverage, associated with wetlands, ranges from 4% to 28% across the seven classes, with the largest coverage in PHT and PGL and the smallest coverage in IG. More details on the classification are provided by Wolfe et al. (2019).

3 Methodology

110 3.1 Virtual basin (VB) based modeling approach

To set up hydrological models in CRHM parsimoniously, the VBs were assigned an area of 100 km², in accordance with the average area of the 4175 Prairie basins classified by Wolfe et al. (2019). Each VB consists of five upland covers of fallow fields, cultivated fields, grasslands, shrublands, woodlands, and three downstream land types of depressions filled with wetlands, open water bodies and stream channels that were used to define HRUs (Spence et al. 2022a and b, Table 1, Figure 2). The HRU
115 area fractions were derived from the results of the basin classification. In each VB except SM, the five upland covers were divided into two portions based on the average effective drainage area of the class (Table 1). The effective part contributes runoff directly to the channel, while the non-effective part routes runoff through a stylized wetland depression complex as shown by HRUs with a suffix of ‘_wd’ in Figure 2a and Table 1. This was not done for SM owing to widespread historical drainage of wetlands in this part of the prairie, with remaining wetlands typically highly modified and lying adjacent to drainage
120 ditches. The depression complex was characterized using 46 ‘wetland’ HRUs (Figure 2a, except SM), with every two upper wetlands contributing to one downstream wetland (Pomeroy et al., 2014). Runoff from the depression complex was routed to

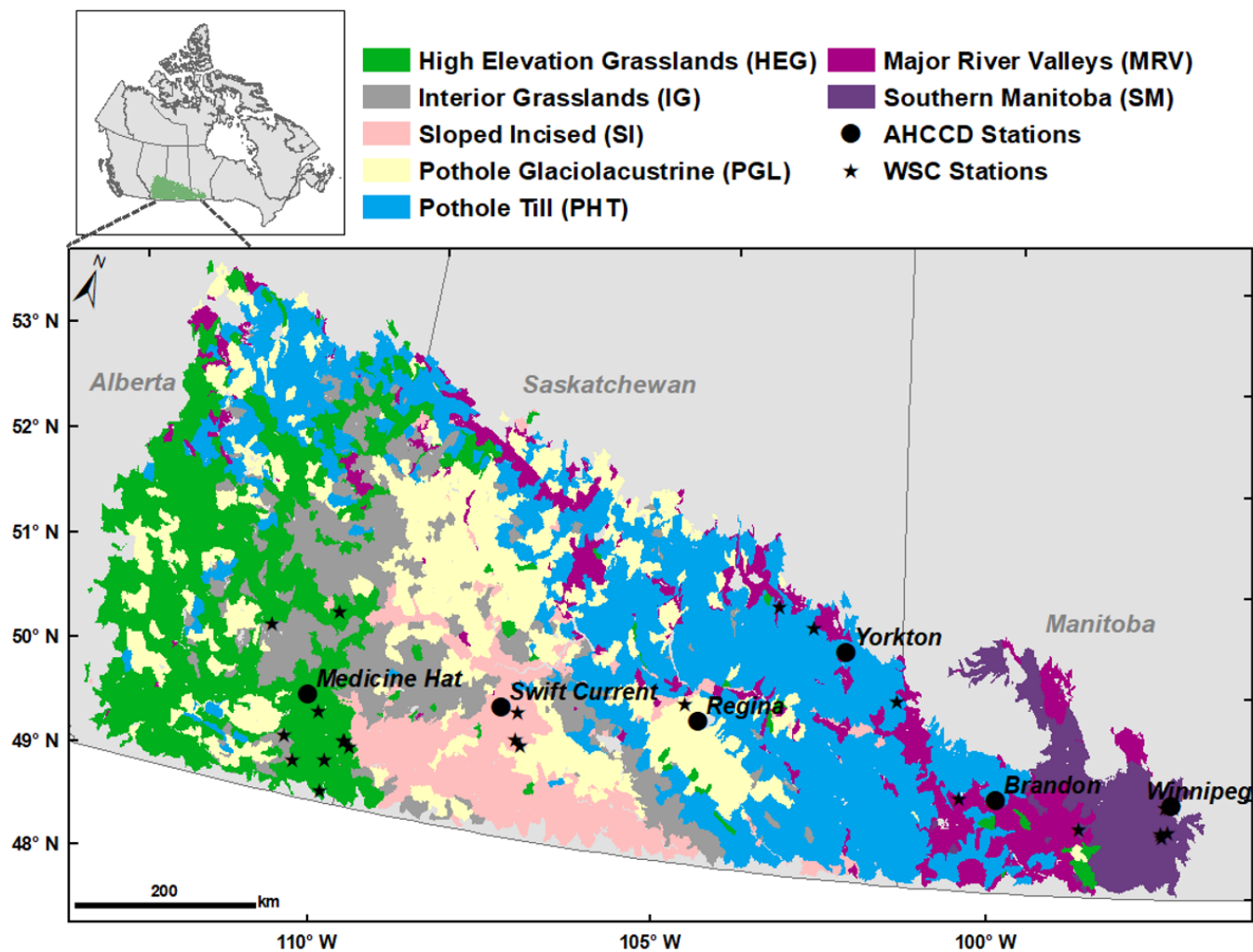


Figure 1. Map of the Prairie ecozone study area in south-central western Canada (inset) with basin classes and locations of AHCCD meteorological stations and Water Survey of Canada (WSC) streamflow stations. Note that areas in light grey are excluded from the analysis (due to large water bodies or urban coverage of the basin, or not being entirely within the study domain).



the bottom openwater HRU and then to the channel HRU. Areas of the 46 ‘wetland’ HRUs were estimated by generalized Pareto distributions using parameters (i.e., β and ξ in Table 1) estimated in Wolfe et al. (2019) for the individual basin classes (Shook et al., 2013).

125 For MRV, a unique valley HRU was inserted between the open water HRU and channel (see dashed lines in the bottom of Figure 2a). Runoff from the effective part was routed to the valley first, and then to the channel HRU, whilst runoff from the depression complex flowed into the openwater HRU first, and then to the valley and to the channel. This HRU represented the incised alluvial valley that is a distinct feature of this basin class. In the SM basins, where warmer and wetter conditions allow a broader diversity of agricultural crops that require specific parameterization, wetlands are typically connected to the
130 channel, much of which has been straightened via ditching. As such, the VB model representing these basins was composed of twelve HRUs (one representing a wetland) with five distinctive crop HRUs (Figure 2b; Table 1), in which HRUs are connected to the channel HRU directly. Fractions of HRUs representing different landcover were determined as described above, with fractions of each crop HRU derived from statistical analysis of land covers in two well-researched basins: South Tobacco Creek (Mahmood et al., 2017) and the La Salle River (Cordeiro et al., 2017) in Manitoba’s Red River Valley

135 3.2 Cold Regions Hydrological Model (CRHM) and model parameterization

The CRHM platform is an object-oriented modeling system with modules representing a wide range of hydrological processes (Pomeroy et al., 2007; 2022). Models created with CRHM have proven successful for simulating streamflow in Canadian Prairie basins (Pomeroy et al., 2007, 2010, 2012, 2014; Fang et al., 2010; Mahmood et al., 2017; Coreiro et al. 2017; 2022), and also in the US northern great plains (Van Hoy et al., 2020). CRHM is strongly physically based and requires no parameter
140 calibration, and so is highly suitable for the VB modeling approach because the VB does not refer to a specific gauged location that can be used for calibration (Pomeroy et al., 2013; Spence et al. 2022a). A suite of modules was chosen to build and run the Prairie VB models in CRHM. The primary modules used were (see more details on modules in Pomeroy et al., 2010): an observation input module to read the meteorological forcing of air temperature, wind speed, relative humidity and precipitation data; a Prairie Blowing Snow module to simulate the blowing snow redistribution and sublimation in the winter based on
145 vegetation height, topography and wind speed; an Energy-Budget Snowmelt module to estimate snowmelt in spring according to the net balance between radiation and conductive and convective heat fluxes; a soil module to represent soil moisture dynamics, infiltration of snowmelt and rain and Hortonian and Dunnian runoff generation, thawing and freezing of soil water, and the filling and spilling of wetland depression storage (Leibowitz and Vining, 2003); an ET module to simulate actual evaporation from unsaturated surfaces using Granger and Gray’s (1990) combination method ET algorithm; Priestley and
150 Taylor’s energy-advection evaporation formula for saturated surfaces and open water bodies; and a routing module using a Muskingum approach to route runoff between HRUs to the basin outlet stream.

The strong physical basis of the CRHM modules allows the parameters to be estimated from field studies described in the literature using the Deduction-Induction-Abduction approach (Pomeroy et al., 2013). For each HRU in the VBs, parameters of vegetation height and leaf area index (LAI) were set to represent the holding capacity of snow accumulation and canopy

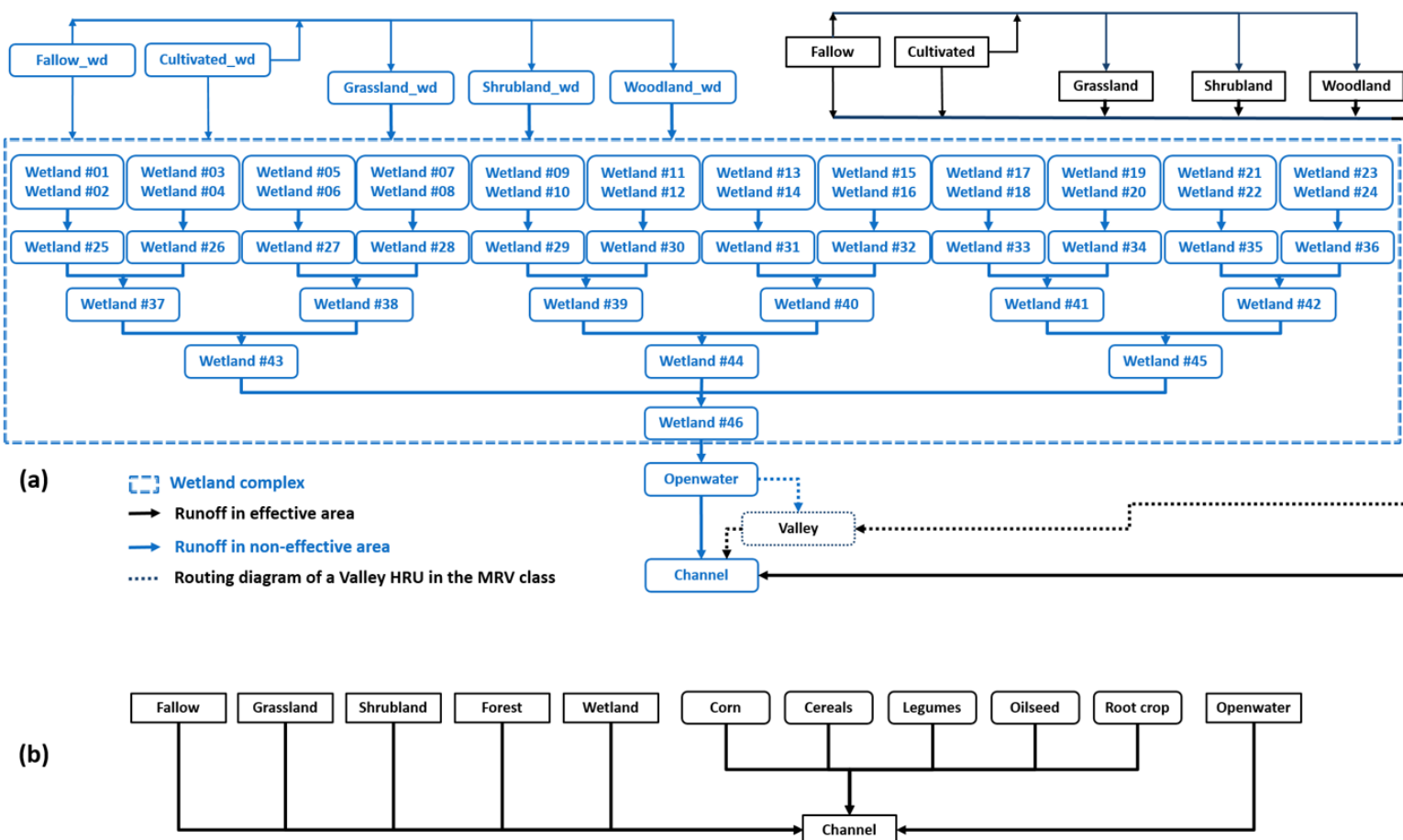


Figure 2. Routing orders of HRUs in the seven VB models created using CRHM. (a) VB models of HEG, IG, PHT, PGL, SI and MRV, where dashed arrow-lines indicate location of the valley HRU in MRV basins; and (b) VB model of SM.



Table 1. HRU fractions for the VB models created by CRHM. The ‘_wd’ notation refers to the fraction that is in the wetland catena. The long-term mean air temperature and mean annual precipitation observed at AHCCD stations are for 1965-2005. Basin-average effective area fraction, routing length and depressional storage capacity, parameters for deriving the wetland distribution, and crop types in the SM VB, as well as IDs of selected WSC stations for model evaluation are listed.

	HEG	IG	SI	PGL	PHT	MRV	SM
HRU fraction							
Fallow	0.004	0.002	0.01	0.002	0.002	0.003	4.9E-06
Fallow_wd	0.002	0.03	0.01	0.01	0.01	0.002	-
Cultivated	0.32	0.04	0.34	0.18	0.18	0.23	-
Cultivated_wd	0.13	0.38	0.15	0.46	0.47	0.17	-
Grassland	0.30	0.04	0.26	0.01	0.02	0.11	0.27
Grassland_wd	0.12	0.40	0.11	0.03	0.06	0.08	-
Shrubland	0.02	0.002	0.01	0.003	0.005	0.04	0.02
Shrubland_wd	0.01	0.02	0.01	0.01	0.01	0.03	-
Woodland	0.02	0.001	0.02	0.002	0.01	0.05	0.10
Woodland_wd	0.01	0.01	0.01	0.01	0.03	0.04	-
Wetlands	0.07	0.04	0.06	0.28	0.21	0.07	0.08
Openwater	1.9E-06	3.4E-02	1.8E-06	3.3E-06	3.7E-06	1.7E-06	0.05
Valley	-	-	-	-	-	0.17	-
Channel	7.2E-03	7.2E-03	6.7E-03	3.0E-03	3.4E-03	9.9E-03	0.005
Effective area fraction	0.67	0.12	0.65	0.19	0.22	0.61	0.92
Mean routing length (m)	6757	7879	6677	6299	6537	5128	6256
Mean depressional storage capacity (mm)	108	105	87	140	182	89	96
Representative AHCCD station	Medicine Hat	Swift Current	Swift Current	Regina	Yorkton	Brandon	Winnipeg
Mean annual T ($^{\circ}\text{C}$)/ P (mm)	5.6/381	3.7/393	3.7/393	2.8/460	1.6/516	2.1/544	2.8/601
IDs of selected WSC stations for model evaluation	05AF010; 11AB902	05CJ011	05JC004	05JF011	05ME007	05MG011	05OG009
	05AH037; 11AB117	05CK005	05JB007		05MB012	05OF011	05MJ009
	011AB111; 11AB081		05JB005		05MA022		05MJ007
	11AA026; 05AH041						05OG010
							05OG003
							05MJ011
Wetland area generalized							
Pareto distribution parameters							
Scale (β)	2121.99	2813.42	2074.92	2195.37	2227.08	1910.83	-
Shape (ξ)	1.15	1.15	1.13	1.19	0.87	1.38	-
Crop HRU parameters in SM							
Crop type	Corn	Cereals	Legumes	Oilseed	Root Crop		
HRU area fraction	0.01	0.26	0.03	0.18	0.003		
Maximum LAI	5	3	3	4.5	3.75		
Vegetation Height (m)	1	1.05	1.04	1	0.55		



155 interception in winter. The vegetation height for grassland and shrubland were set as 0.4 m and 1.5 m, respectively, adopting
from Spence et al. (2022a and b). Heights of crops range from 0.55 m to 1.05 m depending on the crop types (Table 1). The
maximum LAI for grassland and shrubland were set as 3 and 5 (Spence et al. 2022b), and crop LAI in the SM VB ranged from 3
to 5. In addition, a depressional storage capacity was defined to govern the storage and release of water in the wetland complex
(Table 1). Storage capacities of wetlands were estimated based on wetland HRU areas, using logarithmic or linear regression
160 relations derived from LiDAR-measured DEM data (Pomeroy et al., 2014). Soil properties in the HRUs were assumed to be
loam as this was the most common as determined in Wolfe et al. (2019). Routing distances across each HRU to its downstream
HRUs were estimated by a modified Hack's Law length-area relationship that was derived from Smith Creek Research Basin
in Saskatchewan by Fang et al. (2010) (Table 1).

3.3 Model application

165 Historical (1965–2005) meteorological measurements from the Adjusted Homogenized Climate Change Data (AHCCD, Mekis
and Vincent, 2011) served as the baseline climate to force the CRHM-based VB models (Figure 1). This dataset is operated by
Environment and Climate Change Canada's department of Meteorological Service of Canada. Meteorological inputs include
hourly observations of wind speed, relative humidity, surface air temperature, and daily measurement of precipitation which
was corrected for wind-undercatch of snowfall in gauges. To reduce the computational effort, only one representative AHCCD
170 station was chosen to force each class's VB model, selected based on the proximity between the class centroid and the station
location, as well as the availability of gauged meteorological data (Table 1). Based on the long-term mean annual precipitation
at representative AHCCD stations and the area fractions of grassland and cropland HRUs, the seven basin types were divided
into two groups: one is dry and grassland-characterized type including HEG, IG and SI; the other is wet and cropland-dominated
type for PGL, PHT, MRV and SM.

175 Daily streamflow measurements from Water Survey of Canada (WSC) stations that are close to the representative AHCCD
stations and gauge a basin which is >90% in the associated class (see stars in Figure 1 and IDs in Table 1) were selected for the
VB model evaluation phase. As daily streamflows in the Prairies are often zero, except during and following spring snowmelt,
model performance was based on gauged annual and monthly streamflow. Snow depth measurements on cropland taken in the
South Tobacco Creek Research Basin by the WEBs Project of Agriculture and Agri-Food Canada (Mahmood et al., 2017)
180 were used to evaluate the model ability to simulate snow accumulation in the SM class. Performance of the PHT VB model
has proven acceptable in simulating the inter-annual variability of depressional storage by Spence et al. (2022b).

To represent the potential future temperature (T) changes over the Prairies, seven T input scenarios were used to force
the CRHM-based VB models to reflect predictions from an ensemble of climate models for the 21st century. This included
a baseline scenario using historical T observations from the representative AHCCD stations, and six perturbation scenarios
185 with warming from 1 °C to 6 °C with an increment of 1 °C. Five precipitation (P) input scenarios were used to represent
potential future changes in P as reported by Bush and Lemmen (2019) and Johnson et al. (2005): a baseline scenario using
historical P observations from the representative AHCCD stations, a drier scenario assuming that the P will drop by up to 20%



of the baseline observation, and three wetter scenarios with P increasing by 10%, 20% and 30%, respectively. To examine the synergistic impacts of combined P and T perturbations on VB outputs, the five P scenarios were combined with the seven T scenarios, resulting in 35 climate input scenarios.

3.4 Sensitivity analysis

The hydrological variables assessed include annual peak SWE (snow accumulation), annual snowmelt runoff, winter snow sublimation and spring snowmelt infiltration, growing season soil moisture (θ) in the shallow soil (recharge) layer and in the lower soil (deep root) layer, annual and monthly streamflow (Q) at the basin outlet, annual ET, annual maximum connected fraction (CA) and mean daily depressional storage (SD). These variables were evaluated at the basin scale, while snow processes and soil moisture were further assessed for cropland, grassland and wetland HRUs (wetland results were area-weighted across the 46 individual HRUs). All variables except CA have the unit of mm . θ was assessed at a depth range of 0–12 cm for the recharge soil layer and 12–140 cm for the deep root soil layer. A Pearson Correlation Coefficient (CC) between Q sensitivity and the sensitivity of ET, SWE, θ and CA was used to investigate the major underlying contributor for Q sensitivity in the basin types of HEG, IG, SI, PGL, PHT and MRV. To facilitate comparisons between classes, hydrological sensitivity was quantified using the concept of elasticity (Eqs. 1–2). Elasticity (Schaake 1990) is used to assess the climatic sensitivity of hydrological processes, referring to the percent change in a hydrological variable caused by a degree ($^{\circ}C$) warming or by 1% change in P . Recently, Rasouli et al. (2022) used this metric to investigate hydrological sensitivity to climate perturbations in three North American mountainous basins, due to its advantage of standardizing the quantification of sensitivity at different locations. The temperature elasticity (TES) has a unit of $\% \text{ } ^{\circ}C^{-1}$, whilst precipitation elasticity (PES) is dimensionless.

$$TES = [(M - m)/m] \times 100/\Delta T \quad (1)$$

$$PES = [(M - m)/m]/[(P_s - P_b)/P_b] \quad (2)$$

where, ΔT refers to the degree ($^{\circ}C$) change in T , P_s is the P amount in the perturbed scenario, and P_b is the baseline P amount. M is the hydrological variable value forced by perturbed T or P scenarios, and m refers to the corresponding variable value forced by baseline T and P inputs. In this study, as the hydrological models were forced by a range of P and T perturbations, mean PES was thus estimated as slope of the best fit line to scatter plots of $[(P_s - P_b)/P_b, (M - m)/m]$ derived from simulations in the 35 climate input scenarios. Similarly, mean TES was estimated as the slope of the best fit line to scatter plots of $\{\Delta T, [(M - m)/m] \times 100\}$.

4 Results

4.1 Model evaluation

Comparisons in Figure 3 indicate that streamflow simulations by the VB models aligned with observations of little or no streamflow in autumn and winter. The VB models also reasonably simulated that streamflow in the Prairies is dominated by



runoff during snowmelt from March to May. The mean values and ranges of annual streamflow simulated by the VB models
220 reflected observed annual streamflow amounts, especially in the IG and PHT basins. In some cases at monthly scales (HEG
in March to September; other basins except SM in March to April), the VB models underestimated observed streamflow.
Simulated monthly streamflow in SM was slightly larger than observations in April to June.

Bias in simulated monthly and annual streamflow could be caused by two factors. First, the AHCCD meteorological stations
are generally located outside of the basins that were gauged by the selected WSC stations (Figure 1). Meteorological inputs
225 measured at the AHCCD stations are therefore different from those that triggered runoff in the WSC gauged basins. This is most
severe for summer rainfall, where misrepresentations of intense, but small spatial and temporal scale convective rainstorms
occurring in the gauged basins, but missed in the AHCCD precipitation, likely contributed to underestimation of simulated
streamflow in the warm seasons. Second, the CRHM-based VB hydrological models were structured and parameterized using
the median characteristics of each class. The VB model parameters, such as the effective-area fraction and land use type can
230 differ from those in the specific WSC gauged basins, which likely led to some differences between simulated and observed
streamflow.

Simulated snow depth on multiple cropland sites replicated observations well in most years between 2001 and 2011 in the
SM class (Figure 4). Although the model slightly underestimated peak snow depth in 2004 and 2010, observed snow depth in
the remaining years in general fell within the simulation ranges at the various crop HRUs. The simulated snow accumulation
235 showed reasonable pattern that started in October and ended in March when melt and sublimation deplete the snowpack. Snow
cover disappeared from April and May due to strong melting. In addition to the evaluation in SM, the VB model have proven
effective in matching observed SWE at Red Deer, Alberta in the HEG class (Spence et al., 2022a).

Model performance in simulating soil moisture was not evaluated by this work due to limited availability of soil moisture
measurement surrounding the representative AHCCD stations. Instead, CRHM-based VB models were verified as effective
240 in simulating the soil moisture limited ET at Lethbridge, Alberta and Central Saskatchewan (Armstrong et al. 2015). In the
ET algorithm of CRHM, actual ET rate was represented by a function of soil properties and moisture stress (Armstrong et
al. 2010), in which soil wetness was tracked for the ET calculation. Good agreement between cumulative curves of observed
and simulated ET in Armstrong et al., (2010) and (2015) implied that the seasonality of soil moisture could be reasonably
represented in the CRHM VB models. Moreover, the CRHM soil module has proven acceptable in reproducing observed
245 volumetric soil moisture in Smith Creek, Saskatchewan (Fang et al. 2010). Considering that the CRHM-based VB models
were not calibrated against observations and the models were parameterized using typical values in the corresponding classes,
and that they were forced with climate data located at some distance from the monitored sites, results in this and previous
studies implied that the VB models are fit as tools to investigate hydrological sensitivity to climate perturbations in the Prairies.

4.2 Snow sensitivity to climate perturbations

250 Snow elasticity was different among land covers. For example, absolute *TES* of peak SWE in cropland and grassland were
smaller than that in wetlands in all seven basin types, especially in the dry and grassland-characterized basins (Figure 5). In

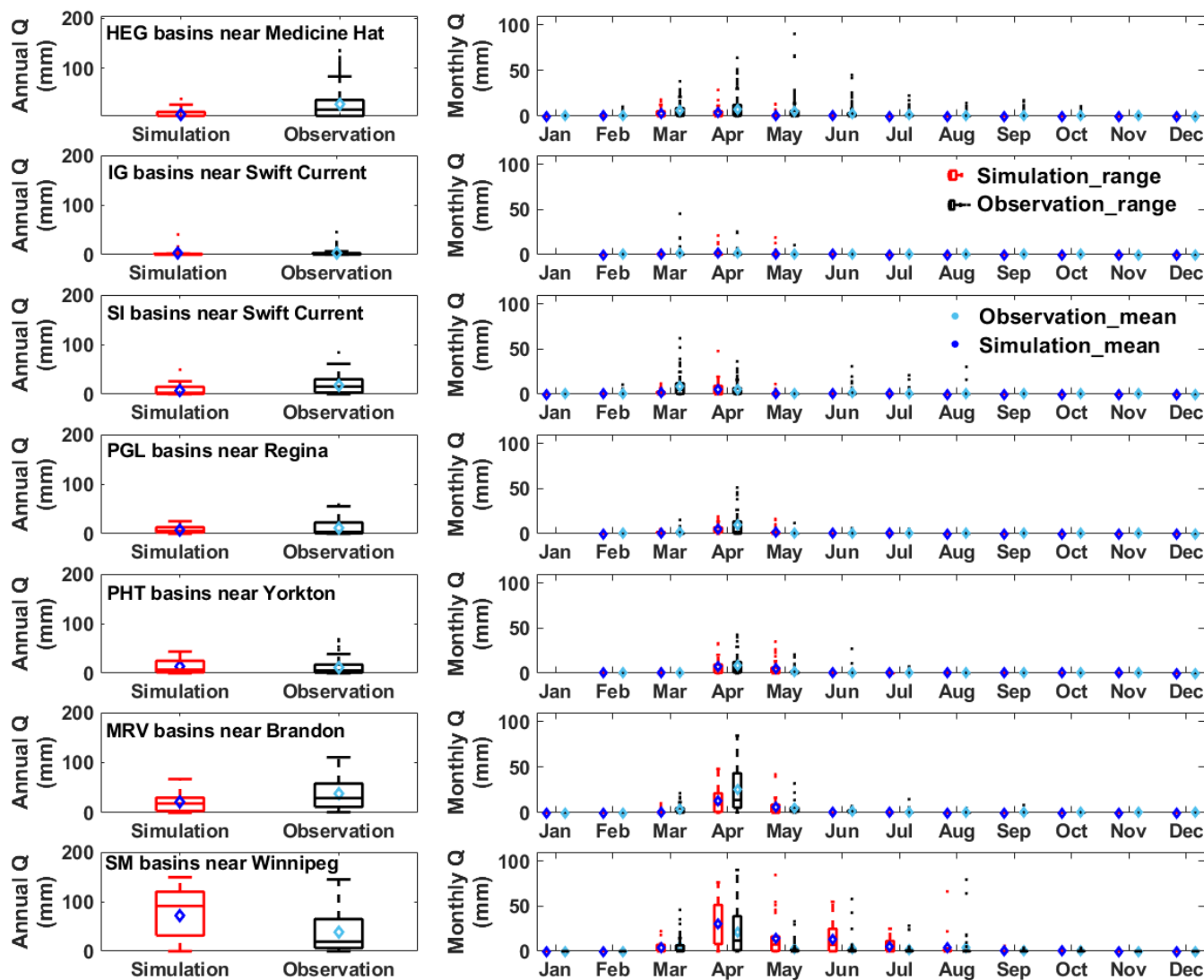


Figure 3. Performance of the CRHM-based hydrological models in simulating annual (left panel) and monthly (right panel) streamflow (Q) over the Prairies (1965–2006). Boxplots refer to the inter-annual variability in streamflow, and diamond dots represent the long-term mean values.

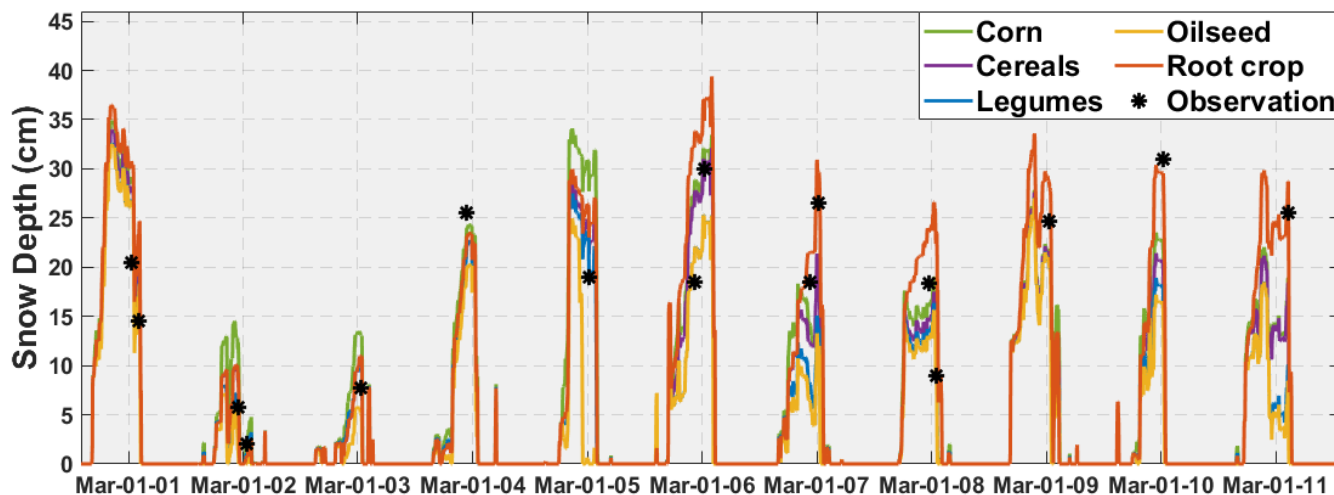


Figure 4. Model performance in simulating snow depth observed at the South Tobacco Creek site in the SM class during 2001–2011.

these classes, mean absolute *TES* of peak SWE in the wetland were around $13 \% \text{ } ^\circ\text{C}^{-1}$, whilst they were only $8\text{--}9 \% \text{ } ^\circ\text{C}^{-1}$ in the cropland and grassland (see gray dots in Figure 5). In the wet and cropland-dominated basins, mean absolute *TES* of peak wetland SWE were around $8 \% \text{ } ^\circ\text{C}^{-1}$, whilst they were only $5\text{--}7 \% \text{ } ^\circ\text{C}^{-1}$ in the cropland and grassland. Absolute *TES* in cropland was smaller than grassland in the grassland-characterized basins and PGL, but larger in the remaining classes. Similarly, mean *PES* of peak SWE in wetland was larger than that in cropland and grassland (except PHT and MRV), especially in SM. The mean *PES* of peak SWE in wetlands was 1.4 in the SM class and close to 1.0 in the remaining classes, whilst both cropland and grassland mean *PES* were lower than 1.0 in all the basin types. Cropland *PES* in the grassland-characterized basins were smaller than grassland, but larger in the cropland-dominated basins. Variability in wetland snow elasticity forced by diverse *P* and *T* inputs was much larger than that in cropland and grassland (Figure 5), partly because snow accumulation in wetlands were strongly influenced by snow redistribution from all upland HRUs, which was sensitive to climate input.

At the basin scale, peak SWE showed decreasing mean absolute *TES* from the drier and grassland-characterized classes to the wetter and cropland-dominated classes, with the largest value of $9.2 \% \text{ } ^\circ\text{C}^{-1}$ in HEG and the smallest value of $7.1 \% \text{ } ^\circ\text{C}^{-1}$ in PHT (Table 2). This could be partly caused by the higher baseline peak SWE of the colder and wetter climates in the cropland-dominated classes (Table 1). Despite that, wetlands showed larger absolute *TES* than other land covers in Figure 5, and wetland fractions in the cropland-dominated classes were larger than those in the grassland-characterized basins (Table 1), results in Table 2 indicated that the *TES* of basin SWE was more determined by local climate rather than land cover characteristics. The other winter snow process of sublimation, was more sensitive to *T* than was SWE, showing the same decreasing tendency from grassland to cropland dominated basins. *TES* for snowmelt runoff and peak SWE were comparable among the grassland-characterized classes, which can be expected as redistributed snow accumulation serves as the primary contributor to melt runoff. However, in the cropland-dominated basins, the *TES* of snowmelt runoff was lower than that of peak

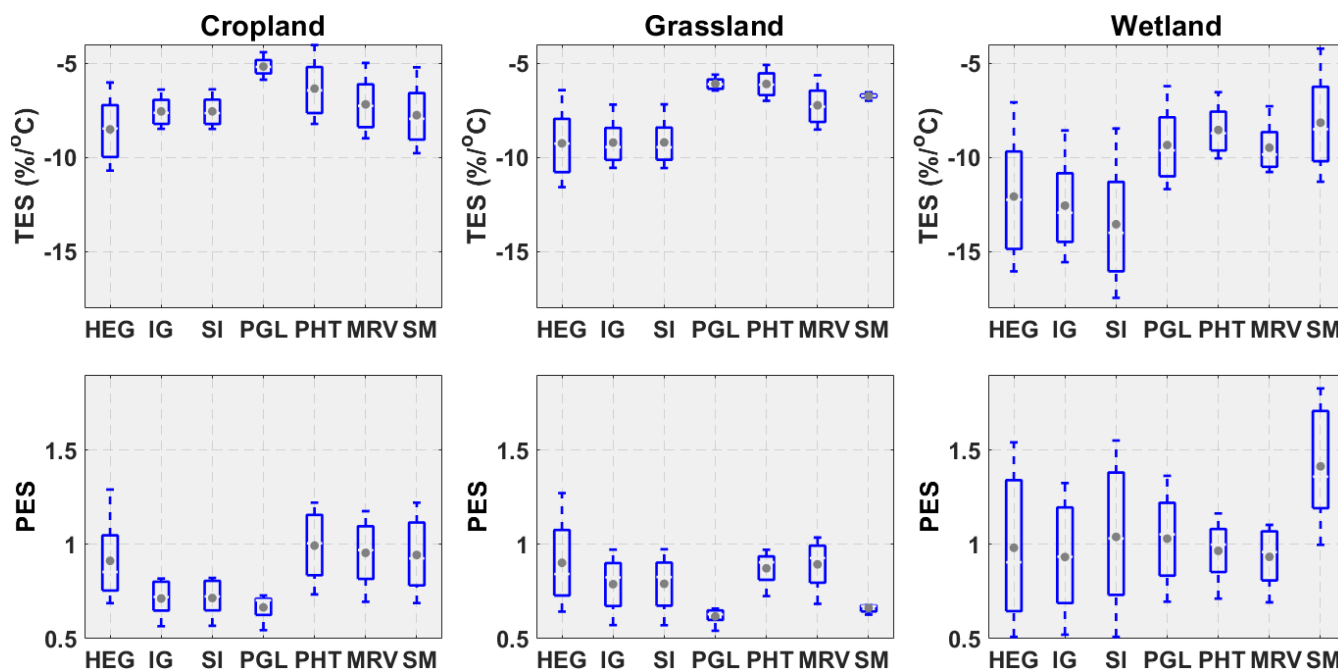


Figure 5. T and P elasticities of annual peak SWE on varied land covers in the seven basin classes. Boxplots are for the inter-annual variability.

Table 2. Mean elasticities of basin-average snow processes/variables to warming and *P* rising forced by 35 climate input scenarios. *TES* and *PES* are for temperature elasticity and precipitation elasticity, respectively.

<i>TES</i> (% °C ⁻¹)	HEG	IG	SI	PGL	PHT	MRV	SM
Peak SWE	-9.2	-8.9	-9.0	-7.3	-7.1	-7.6	-7.8
Snow sublimation	-18.1	-15.3	-16.2	-10.8	-10.6	-10.7	-9.1
Snowmelt runoff	-9.6	-9.7	-10.0	-5.4	-3.1	-4.9	-5.9
Snowmelt infiltration	-2.6	-1.8	-1.7	-4.6	-9.2	-5.7	-4.0
<i>PES</i>							
Peak SWE	0.9	0.8	0.8	0.8	1.0	0.9	0.9
Snow sublimation	1.4	1.3	1.4	1.4	1.0	1.0	0.8
Snowmelt runoff	1.2	1.1	1.2	1.1	1.2	1.3	1.1
Snowmelt infiltration	0.3	0.3	0.3	0.1	0.2	0.1	0.1

SWE, which could be attributed to the large *TES* of snowmelt infiltration (Table 2). The strong decrease in snowmelt infiltration in these classes could partly offset the decrease in snowmelt runoff caused by warming.

PES of snow sublimation was larger than 1.0 in the dry and grassland-characterized classes and PGL (Table 2), which indicated that snow sublimation was limited by snowfall availability in these classes. When *P* increased and generated more

275

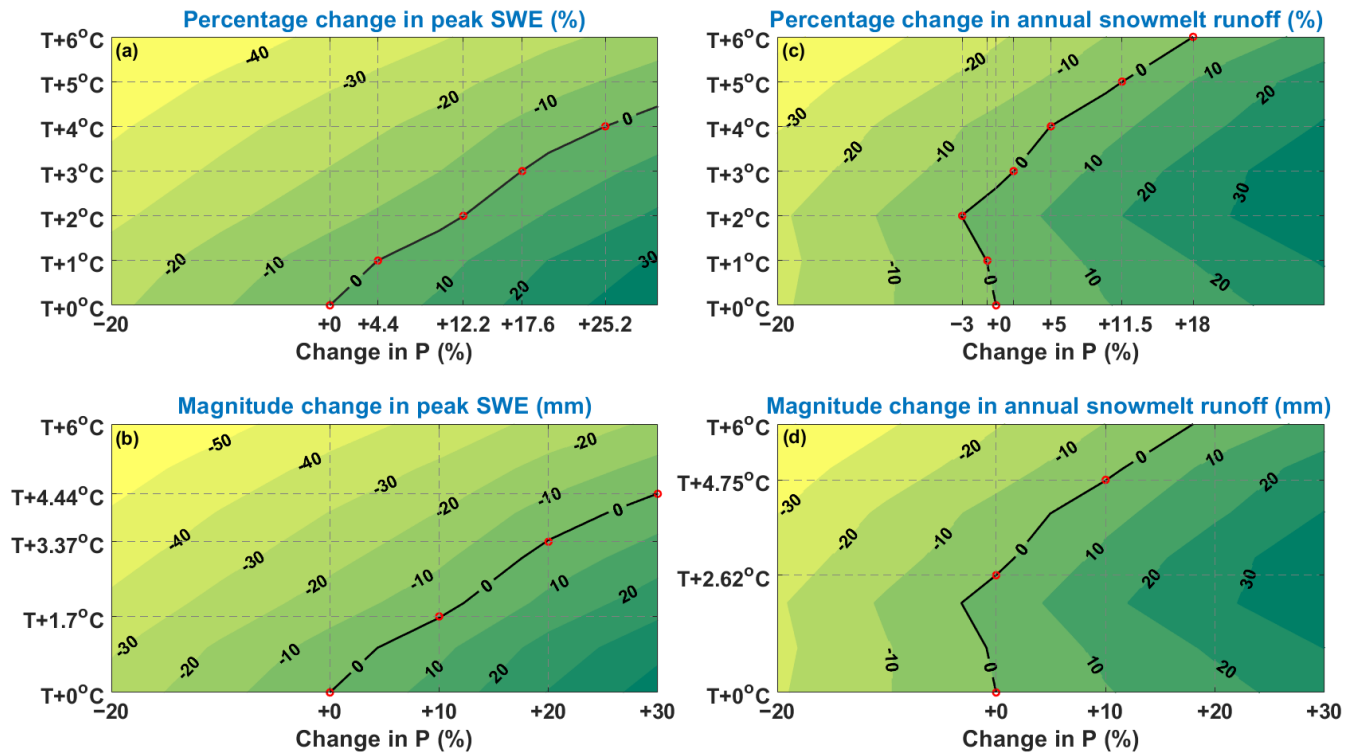


Figure 6. Combined effects of T and P perturbations on annual peak SWE and snowmelt runoff in the PHT class. Red dots on the upper panel show where the effects of warming scenarios were offset by percentage changes in P , and those on the lower panel show where the effects of P rising scenarios were offset by warming degrees in T .

snowfall, sublimation showed a larger percentage increase rate than P . This could explain why PES of peak SWE was lower than 1.0, because of the enhanced snow loss via sublimation. In contrast, snowmelt infiltration was controlled by the rate of soil thawing associated with T in the melting season rather than the availability of snow meltwater in the Prairie basins. Although increased P resulted in larger snowmelt, PES of snowmelt infiltration was smaller than 1.0 because of the restriction by frozen soil. As a result, PES of snowmelt runoff was larger than 1.0 because of the increased snowmelt availability for surface runoff generation (Table 2). Compared to TES , PES of snow processes showed smaller variations across the seven classes.

Effects of expected warming on peak SWE (i.e., percentage and magnitude changes in SWE caused by warming) can be partially offset by increased P within its possible future range in the Canadian Prairies. Using the results from the PHT class as an example (because this basin class has the largest areal extent among the seven classes), decreases in peak SWE caused by warming from 1 °C to 4 °C can be completely offset by the gains from P increases ranging from 4.4% to 25.2% (Figure 6a). The maximum expected increase of 30% in future P , however, cannot fully offset the decrease in SWE caused by warming higher than 5 °C. On the other hand, increases in SWE associated with P increases of 10%, 20% and 30% can be offset by warming of 1.7 °C, 3.37°C and 4.44°C, respectively (Figure 6b). With warming of 6 °C, the decreases in snowmelt runoff can

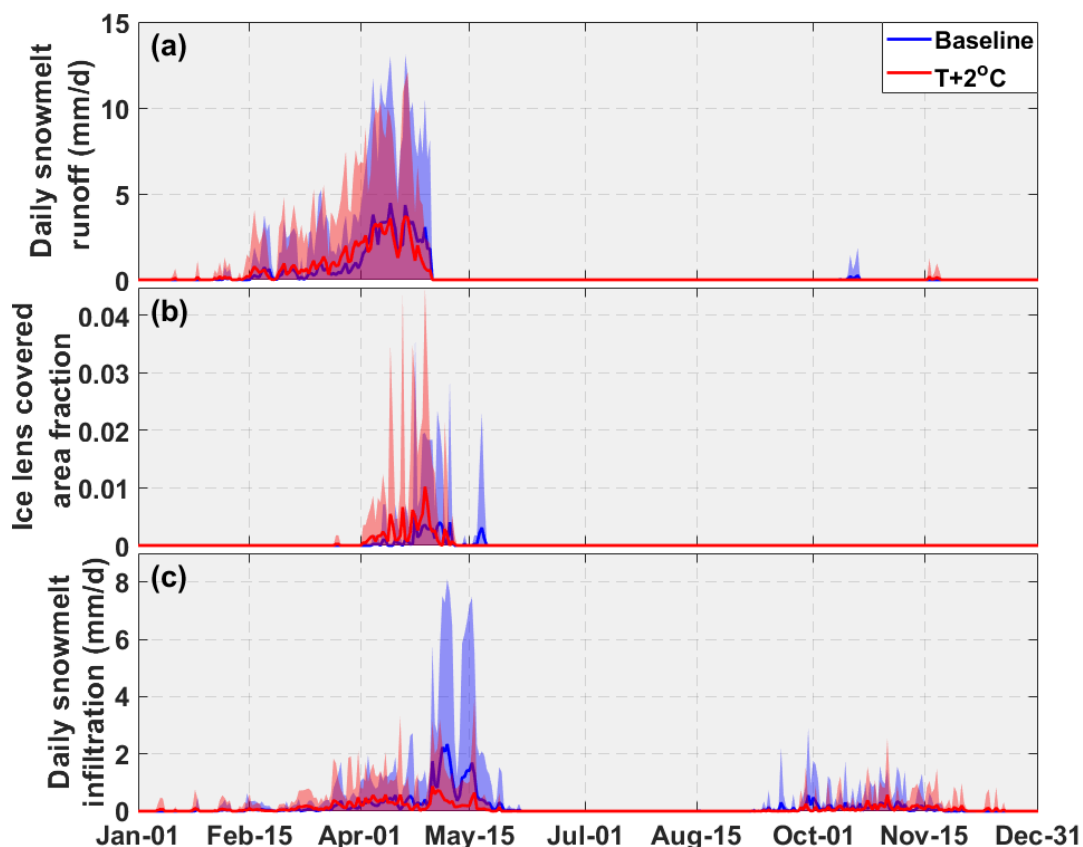


Figure 7. Comparisons of daily snowmelt runoff, ice lens covered area fraction, and daily snowmelt infiltration in two T scenarios in the PHT class. Bands refer to the inter-annual variability, and solid lines are for the mean values during the modeling period.

be fully offset if P increases by 18% (Figure 6c). On the other hand, offsetting the increase in snowmelt runoff created with a
290 P increase of 10% requires warming of 4.75 °C (Figure 6d). P increases greater than 20% cannot be fully offset by warming
lower than 6 °C.

It is noted that snowmelt runoff increases with warming of 1–2 °C in the PHT class (Figures 6c-d). This phenomenon could be
caused by restricted snowmelt infiltration with warming, when ice lenses can form from spring melts preceding full snowmelt
(Figure 7), and more rain-on-snow events in warming scenarios (Fang and Pomeroy, 2007; Mahmood et al. 2017). With 2 °C
295 warming, snowmelt runoff in March was larger than the baseline runoff due to raised T (Figure 7a). In April, warming resulted
in more ice lenses due to early melting and rain (Figure 7b). Snowmelt infiltration was thus strongly restricted in the warming
scenario (Figure 7c). Therefore, effects of warming of 1–2 °C on snowmelt runoff would be enhanced by P rising but be offset
by P decreases up to 3% (Figure 6c).

The effectiveness of P to compensate for warming effects on peak SWE increased from the drier and grassland-characterized
300 classes to the wetter and cropland-dominated classes (Table 3). To offset the effects of warming by 1 °C, 9.5–10.2% increases



Table 3. Required P increases (%) to offset the effects of warming [or required warming degrees ($^{\circ}\text{C}$) to offset P rising] on annual peak SWE, and the maximum increase and decrease (percentage/magnitude) in peak SWE caused by the 35 combined P and T perturbation scenarios

Required P to offset warming (%)	HEG	IG	SI	PGL	PHT	MRV	SM
$T +1^{\circ}\text{C}$	+10.2	+9.5	+9.8	+6.4	+4.4	+4.6	+4.3
$T +2^{\circ}\text{C}$	+22.9	+22.8	+23.2	+13.5	+12.2	+12.7	+15.5
$T +3^{\circ}\text{C}$	>+30	>+30	>+30	+23.0	+17.6	+20.5	+24.5
$T +4^{\circ}\text{C}$	>+30	>+30	>+30	>+30	+25.2	>+30	>+30
$T +5^{\circ}\text{C}$	>+30	>+30	>+30	>+30	>+30	>+30	>+30
$T +6^{\circ}\text{C}$	>+30	>+30	>+30	>+30	>+30	>+30	>+30
Required T to offset P rising ($^{\circ}\text{C}$)							
$P -20\%$	NA	NA	NA	NA	NA	NA	NA
$P +10\%$	+0.96	+1.05	+1.01	+1.5	+1.7	+1.64	+1.52
$P +20\%$	+1.8	+1.8	+1.76	+2.78	+3.37	+2.92	+2.55
$P +30\%$	+2.62	+2.56	+2.56	+3.62	+4.44	+3.93	+3.62
Maximum increase in SWE (%/mm)	40.9/26.2	29.6/17.0	30.3/17.6	32.7/29.5	37.5/44.4	35.3/42.6	34.1/35.0
Maximum decrease in SWE(%/mm)	-62.4/-39.9	-61.2/-35.2	-61.4/-35.7	-50.9/-45.8	-51.4/-60.8	-53.9/-65.1	-56.6/-58.3

in P were required in the HEG, IG, and SI classes, whilst smaller increases of around 4.4% were required in the PHT, MRV, and SM classes. Meanwhile, P increase of 30% would be able to offset the effects of warming up to 3 $^{\circ}\text{C}$ in the PGL, MRV, and SM classes and even 4 $^{\circ}\text{C}$ in the PHT class, whilst such an increase in P could only offset the effects of warming of up to 2 $^{\circ}\text{C}$ in the HEG, IG, and SI classes. In contrast, warming of around 1 $^{\circ}\text{C}$ can offset the effects of a 10% increase in P in the HEG, IG, and SI classes, whilst warming of higher than 1.5 $^{\circ}\text{C}$ is required in the PGL, PHT, MRV, and SM classes.

The 35 combined climate inputs resulted in varied decreases and increases in peak SWE across the basin types (Table 3). The maximum percentage increases in peak SWE due to increased P of 30% were around 30–41% over the entire region, whilst the maximum absolute increases ranged from 17 mm in IG to 44 mm in PHT. The maximum percentage decreases in peak SWE ranged from 51% to 62%, associated with warming of 6 $^{\circ}\text{C}$ and 20% decrease in P ; absolute decreases in this scenario ranged from 35 mm in IG to 65 mm in MRV.

4.3 Soil moisture sensitivity to climate perturbations

Growing season (May to September) soil moisture TES differed among land cover types in the basin classes (Table 4). SM basins were excluded from this analysis, because the VB model performance in simulating soil moisture in the eastern wet area has not been evaluated. Cropland soil moisture showed smaller mean absolute TES than in grassland and wetland along all the six classes. The maximum absolute TES for cropland soil moisture happened in PHT as 3.2 $\% \text{ }^{\circ}\text{C}^{-1}$ followed by 2.5 $\% \text{ }^{\circ}\text{C}^{-1}$ in MRV. TES of grassland soil moisture was slightly higher, with maximum absolute value of 4.6 $\% \text{ }^{\circ}\text{C}^{-1}$ in PHT. Wetland soil moisture showed the largest absolute TES among the land covers with the maximum of 9.3 $\% \text{ }^{\circ}\text{C}^{-1}$ in SI and the minimum



Table 4. Mean elasticities of growing season soil moisture (θ) to warming and P rising derived from simulations in 35 climate forcing scenarios.

TES (% $^{\circ}\text{C}^{-1}$)	HEG	IG	SI	PGL	PHT	MRV
θ in cropland	-2.4	-1.9	-1.9	-1.0	-3.2	-2.5
θ in grassland	-3.1	-2.8	-3.0	-2.6	-4.6	-2.6
θ in wetland	-9.2	-8.9	-9.3	-7.9	-7.8	-8.3
Basin-average θ	-3.4	-3.0	-3.0	-3.8	-4.8	-4.3
PES						
θ in cropland	1.5	1.8	1.8	1.8	1.9	1.6
θ in grassland	1.3	1.6	1.6	1.5	1.8	1.1
θ in wetland	1.8	1.3	1.6	1.6	1.7	1.4
Basin-average θ	1.4	1.5	1.6	1.6	1.8	1.6

of 7.8 % $^{\circ}\text{C}^{-1}$ in PHT. This could be explained by the fact that when their depressional storage dropped to zero, wetlands transitioned to bare surface, and soil moisture under those conditions was thus highly sensitive to warming. Variations in TES of the basin-average soil moisture among the basin types can be explained by the different land cover fractions in the classes (Table 1). For instance, HEG, IG and SI have high coverage of grassland; TES of basin-average soil moisture (around 3.2 % $^{\circ}\text{C}^{-1}$) in these classes was thereby close to that of grassland soil moisture (around 3.0 % $^{\circ}\text{C}^{-1}$). In contrast, PGL and PHT had large land cover fractions of cropland and wetland, and their basin-average soil moisture TES (around 4.3 % $^{\circ}\text{C}^{-1}$) was intermediary to values for cropland (1–3.2 % $^{\circ}\text{C}^{-1}$) and wetland (7.9 % $^{\circ}\text{C}^{-1}$).

PES of growing season soil moisture, however, only exhibited slight differences across land covers and were typically larger than 1.0 which can be attributed to rainfall infiltration in the growing season being limited by the availability of rain input. In all the six classes, PES of cropland soil moisture ranged only from 1.5 to 1.9, and were between 1.1–1.8 and 1.3–1.8 in grasslands and wetlands, respectively (Table 4). Again, basin-average soil moisture PES was close to that of grassland soil moisture in HEG, IG and SI, and was intermediary to values for cropland and wetland in the PGL, PHT and MRV classes.

Moisture in shallow soil layers is of great interest to agricultural producers in the Canadian Prairies and is the source of crop growth by supplying water for dryland farming ET and plant productivity. As expected, moisture in shallow soils (Figures 8a,b) showed smaller mean absolute TES and PES than in deeper soils (Figures 8c,d), because the shallow layer soil moisture capacity is much smaller and receives infiltrating waters first. Despite that, the shallow layer soil moisture mean TES (absolute) and PES generally increased from the drier and grassland-characterized classes to the wetter and cropland-dominated classes, likely because that soil moisture in the shallow layer was easily depleted by ET in the dry sites. Deeper layer soil moisture response showed wide variability among the basin types. It had the largest absolute mean TES of around 4 % $^{\circ}\text{C}^{-1}$ in the PHT class, whilst presenting the largest mean PES of 2.2 in the SI class.

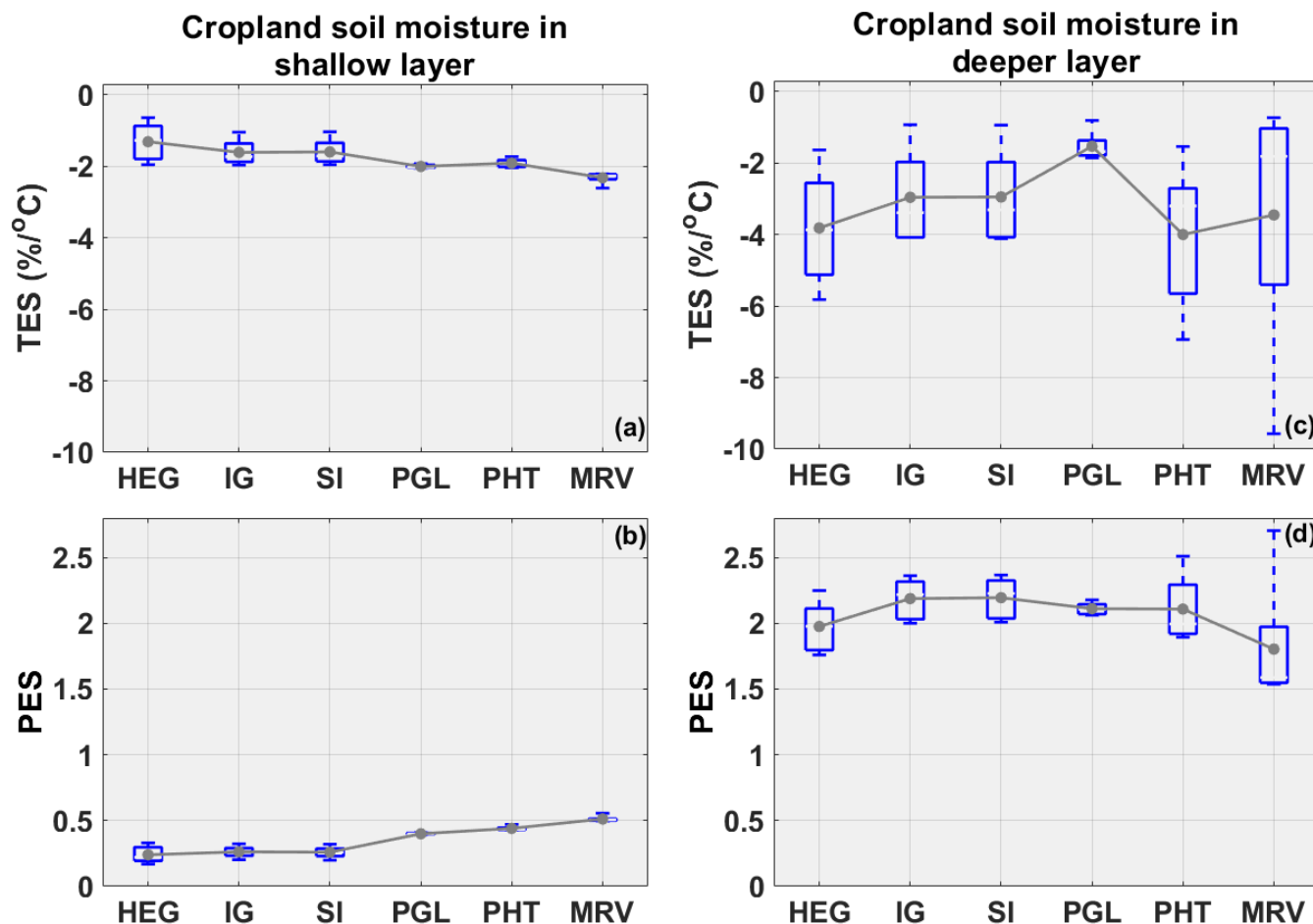


Figure 8. Comparisons of the climate elasticities of mean growing season soil moisture in cropland. Boxplots refer to the variability forced by different P or T inputs, and dot-lines stand for the mean elasticities.

The effectiveness of P in compensating for the effects of warming on cropland's growing season soil moisture showed that a P increase of 10.5% was required to offset the effects of 6°C warming in the HEG and PHT classes, which is much higher than the required increase of 5.4% in the PGL class (Table 5). P increase in the IG and SI classes showed similar effectiveness, offsetting effects of 1°C and 6°C warming with increases of 2.0% and 7.7%, respectively. MRV showed reduced effectiveness compared to IG and SI, indicated by the required P increases of 2.8%, and 7.8% to offset the effects of warming by 1 °C and 6 °C, respectively. In contrast, warming is not effective in compensating for the increases in soil moisture caused by more P . The maximum warming of 6 °C could only offset the effects of P increases up to 11% in any basin types. The maximum percentage increases in soil moisture by 30% P increase approached 61% in PGL, to as large as 110% in MRV. Maximum magnitude increases ranged from 95 mm to 242 mm in all basin types. The maximum decrease in soil moisture forced by 6 °C warming and 20% P decrease showed the percentage and magnitude values of 24–52% and 46–147 mm, respectively.



Table 5. Required P increases (%) to offset the effects of warming [or required warming degrees ($^{\circ}\text{C}$) to offset P rising] on cropland's growing season soil moisture, and the maximum increase and decrease (percentage/magnitude) in growing season's soil moisture caused by the 35 combined P/T perturbation scenarios.

Required P to offset warming (%)	HEG	IG	SI	PGL	PHT	MRV
$T +1^{\circ}\text{C}$	+1.3	+2.1	+2.0	+1.6	+3.3	+2.8
$T +2^{\circ}\text{C}$	+3.2	+3.1	+2.8	+2.8	+7.1	+5.7
$T +3^{\circ}\text{C}$	+5.0	+4.1	+4.0	+3.9	+7.7	+5.8
$T +4^{\circ}\text{C}$	+7.2	+5.5	+5.3	+4.6	+9.5	+7.2
$T +5^{\circ}\text{C}$	+9.6	+7.2	+6.8	+5.0	+9.7	+7.9
$T +6^{\circ}\text{C}$	+10.5	+7.7	+7.7	+5.4	+10.4	+7.8
Required T to offset P rising ($^{\circ}\text{C}$)						
$P -20\%$	NA	NA	NA	NA	NA	NA
$P +10\%$	+5.5	>+6	>+6	>+6	+5.5	>+6
$P +20\%$	>+6	>+6	>+6	>+6	>+6	>+6
$P +30\%$	>+6	>+6	>+6	>+6	>+6	>+6
Maximum increase in soil moisture (%/mm)	69.9/94.8	69.1/113.1	69.5/112.7	61.4/125.1	72.7/207.6	110.4/242.4
Maximum decrease in soil moisture (%/mm)	-34.1/-46.3	-37.2/-60.9	-37.1/-60.1	-40.6/-82.7	-51.6/-147.3	-24.1/-52.8

4.4 Streamflow sensitivity to P and T perturbations

Absolute mean TES and PES of streamflow were much larger than those of snow and soil moisture (Table 6). Mean annual streamflow in the IG class was the most T sensitive at $-31.2\% \text{ } ^{\circ}\text{C}^{-1}$. The SM class showed the smallest absolute TES for streamflow at $6.0\% \text{ } ^{\circ}\text{C}^{-1}$. Streamflow TES (absolute) in the remaining classes were typically around $17\% \text{ } ^{\circ}\text{C}^{-1}$. Similarly, IG had the largest streamflow PES of 5.4, followed by PHT with a PES of 4.5. Streamflow in SM showed comparable PES to that in MRV and PGL, whilst HEG and SI had the smallest PES of 2.3.

Apart from snowmelt contributions, streamflow in Prairie basins is controlled by ET and CA, the latter of which is determined by the state of SD which is most often filled by spring snowmelt. ET increased with both warming and P rising, as shown by its positive TES and PES (Table 6). TES of ET was highest in the wetter and cropland-dominated classes, whilst PES of ET was highest in the grassland-characterized classes, because ET in the drier and grassland-characterized classes was more strongly limited by water availability but more limited by energy input in the wet and cropland-dominated classes. Therefore, PES of ET were around 1.0 in the grassland-characterized classes but lower than 1.0 in the cropland-dominated classes, especially in the SM basins. Basin-average SD in PHT showed the largest mean TES and PES among the basin types, partly because of its largest depressional storage capacity (Table 1). CA over the Prairies showed less sensitivity to P changes than ET, indicated by the PES values of only 0.01–0.4, which means the P input scenarios were not able to strongly change the fill-spill patterns of large depressions in the Prairies; whilst CA in classes of IG, PGL, PHT, and MRV showed visible sensitivity to T change



Table 6. Mean elasticities of streamflow, ET, depressional storage (SD), and maximum connected area (CA) to T and P perturbations derived from the 35 climate input scenarios.

TES ($\% \text{ } ^\circ\text{C}^{-1}$)	HEG	IG	SI	PGL	PHT	MRV	SM
Annual streamflow	-16.5	-31.2	-15.3	-14.0	-21.8	-15.5	-6.0
Annual ET	0.7	0.7	0.8	0.9	1.2	1.2	2.1
Annual mean SD	-7.5	-10.2	-6.8	-5.5	-15.6	-2.9	0.1
Annual maximum CA	-0.1	-3.2	-0.2	-1.2	-1.8	-1.1	0.0
<i>PES</i>							
Annual streamflow	2.4	5.4	2.2	3.2	4.5	4.0	3.6
Annual ET	1.0	1.0	1.0	0.9	0.9	0.8	0.4
Annual mean SD	1.5	1.5	1.3	1.3	3.0	1.2	2.7
Annual maximum CA	0.01	0.4	0.02	0.3	0.4	0.3	0.0

with absolute TES values comparable to that of ET, which can be explained by the fact that enhanced ET by warming strongly
 365 reduced SD in small wetland HRUs and their connectivity to the basin outlet. CA in the SM class showed no sensitivity to
 P and T perturbations because all upper HRUs were connected to the channel in this class (Figure 2b). These show that the
 climate sensitivity of ET, basin water storage and connectivity is greatly exceeded by that of streamflow generation. This is to
 be expected in a semi-arid to sub-humid climate where streamflow is intermittent and small in the baseline scenario.

Correlation Coefficient (CC) between the climate elasticities of annual streamflow and other hydrological variables indicated
 370 that the responses of annual streamflow to climate were mainly related to the response of CA in the wetland-characterized
 basins of HEG, IG, SI, PGL, PHT and MRV (Figure 9). The SM class was not included in this analysis because of its high
 connectivity. Climate elasticities of annual streamflow in SM should be mainly controlled by ET. CC between TES of annual
 streamflow and CA was as high as 0.88, and that for PES was 0.91. Correlations between the climate elasticities of annual
 375 streamflow and other variables including ET, SWE, and basin-average soil moisture were typically lower and not significant
 (at the 5% level). For example, PES of ET and SWE showed small variations among the basin types, which differed from the
 considerable variations of streamflow PES .

The effectiveness of increasing P in compensating for decreases in mean annual streamflow caused by warming increased
 from the grassland-characterized classes to the cropland-dominated classes (Table 7). For example, around a 20% increase in
 P was required to offset the effects of warming by 3 $^\circ\text{C}$ in HEG, whilst in SM, only up to 5% increase in P was required.
 380 Meanwhile, effects of the maximum warming of 6 $^\circ\text{C}$ can be fully offset by P increases up to 30% in PGL, PHT, MRV, and
 SM, whilst 30% increases in P could only offset the effects of warming of 4–5 $^\circ\text{C}$ in HEG and SI. As expected, higher levels of
 warming were required to offset the effects of the same P increases in the cropland-dominated classes. The maximum warming
 of 6 $^\circ\text{C}$ can only offset the effects of P increase of up to 20% in the cropland-dominated classes but can fully offset the effects
 of the maximum increase of 30% in the HEG and SI classes. The maximum increases in mean annual streamflow forced by

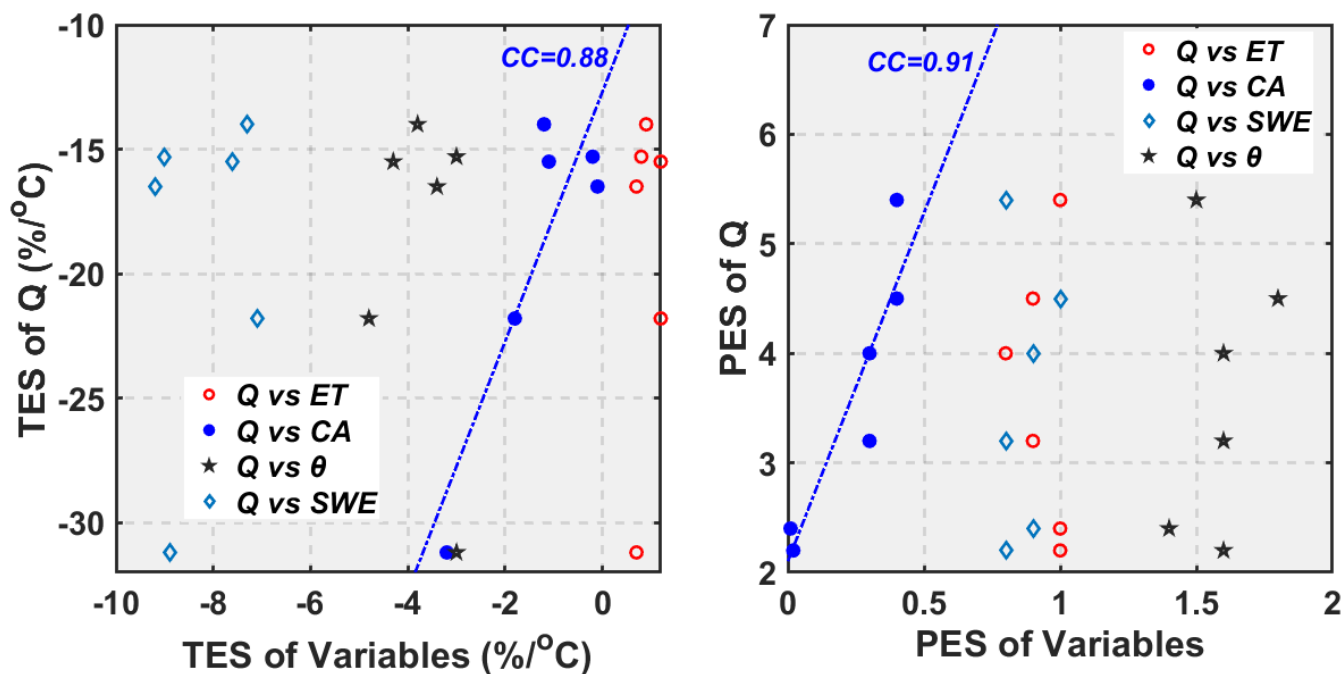


Figure 9. Correlations between climate elasticities of annual streamflow (Q) and other variables in the basin types except SM. CC means the Pearson correlation coefficient, and θ means the basin-average soil moisture.

Table 7. Required P increases (%) to offset the effects of warming [or required warming degrees ($^{\circ}\text{C}$) to offset P rising] on annual streamflow, and the maximum increase and decrease (percentage/magnitude) in mean annual streamflow forced by the 35 combined P/T perturbation scenarios.

Required P to offset warming (%)	HEG	IG	SI	PGL	PHT	MRV	SM
$T +1^{\circ}\text{C}$	+5	+4.0	+3.8	+1.4	+2.4	-1.5	+1.5
$T +2^{\circ}\text{C}$	+12.4	+7.7	+10.2	+5.6	+4.1	-1.0	+3.5
$T +3^{\circ}\text{C}$	+19.4	+14.2	+18.8	+8.4	+9.1	+3.2	+4.8
$T +4^{\circ}\text{C}$	+25.9	+15.7	+23.9	+13.1	+13.8	+6.7	+6.3
$T +5^{\circ}\text{C}$	>+30	+17.8	+27	+15.9	+17.9	+12.4	+7.9
$T +6^{\circ}\text{C}$	>+30	+27.7	>+30	+22.0	+23.5	+18.3	+9.1
Required T to offset P rising ($^{\circ}\text{C}$)							
$P-20\%$	NA	NA	NA	NA	NA	NA	NA
$P+10\%$	+1.6	+2.32	+1.98	+3.3	+3.14	+4.56	>+6
$P+20\%$	+3.12	+5.16	+3.26	+5.7	+5.38	>+6	>+6
$P+30\%$	+4.65	>+6	+5.3	>+6	>+6	>+6	>+6
Maximum increase in annual streamflow (%/mm)	127/11	483/12	118/10	185/16	319/54	234/55	140/150
Maximum decrease in annual streamflow (%/mm)	-91/-8	-98/-2	-92/-8	-78/-7	-81/-14	-85/-20	-73/-78

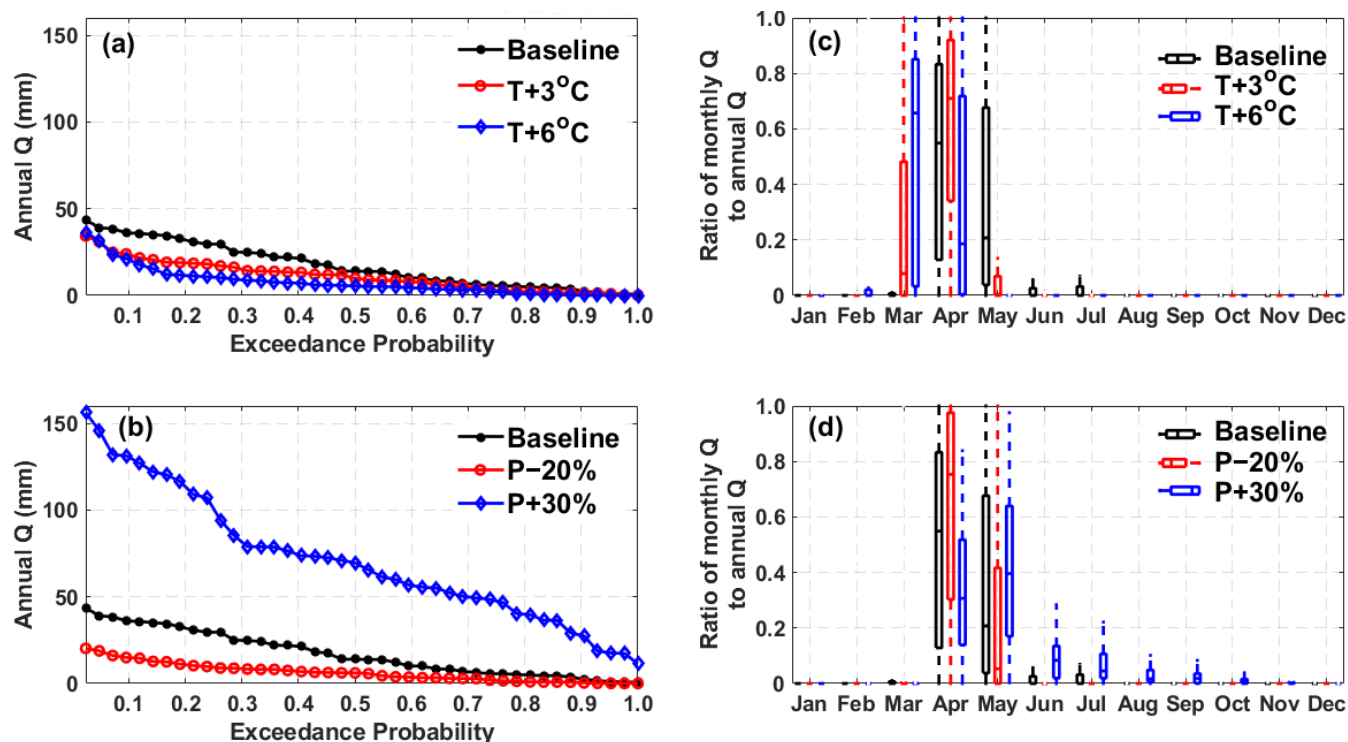


Figure 10. Changes in flow duration curve of annual streamflow (Q) during the modeling period (1965–2005) and the ratio of monthly Q to annual Q under T and P perturbation scenarios in the PHT class. Boxplots refer to the inter-annual variability during the modeling period.

385 the 35 combined P and T scenarios ranged from 118% to 483% and 10 mm to 150 mm, whilst the maximum decreases ranged from -73% to -98% and -2 mm to -78mm.

In addition to the long-term mean annual streamflow, T and P changes showed different impacts on extreme annual streamflow during the modeling period. Taking the PHT class as an example, warming caused larger magnitude reductions in annual streamflow with exceedance probability of 0.1–0.4 than those in peak and extremely low annual streamflow (Figure 10a); whilst P changes resulted in larger changes in peak annual streamflow (Figure 10b). Compared to maximum warming of 6°C, the maximum 30% increase in P caused greater increases not only in extreme annual streamflow but also in those with exceedance probability of 0.1–0.4. The ratio of monthly streamflow to annual streamflow showed considerable switches under T and P perturbation scenarios. With warming of 3–6°C, the dominant period of monthly streamflow on annual streamflow switched from April–May to March–April (Figure 10c). Under 6°C warming, streamflow in March became the major contributor to annual streamflow, whilst that in May became very small. In contrast, streamflow in April–May will remain dominant on annual streamflow within the P change range from -20% to +30% (Figure 10d). P changes won't increase the contribution of March streamflow to annual streamflow, whilst dry scenario (P -20%) considerably enhanced the contribution of April. In the

395



wet scenario ($P+30\%$), contributions from streamflow in June, July, August and September to annual streamflow will be more visible.

400 5 Discussion

5.1 Basin hydrological sensitivity to climate changes

These modeling results are consistent with previous studies that focused on the impacts of warming (e. g., St-Jacques et al., 2018; Tanzeeba and Gan, 2012), which indicate earlier spring runoff, decreased mean annual streamflow and lower peak SWE in the Prairies. Johnson and Poiani (2016) found that a 20% increase in P could strongly offset the effects of 3 °C warming on the wetland water storage in the Prairie Pothole Region, which is similar to the findings here of the combined effects of P and T in the PGL and PHT classes (Table 3). Results from the Bad Lake basin in southwestern Saskatchewan (Fang and Pomeroy, 2007) indicated that spring streamflow would decrease by 20% if air temperature increased by 1°C, and decrease by 1.6% in response to 1% decrease in precipitation, which is rather close to the findings for the HEG and SI (in which Bad Lake basin lies) classes (Table 6). In this study we also showed that annual streamflow showed a larger PES than did SWE, which is consistent with behaviour of Canadian mountain basins to the west of our study region (Rasouli et al. 2022). However, the absolute TES of streamflow over all the Prairie classes were larger than that of peak SWE, which is different from the findings of Rasouli et al. (2022). Reasons for this can be that streamflow in the Prairies are typically dominated by snowmelt in spring with small contribution from rainfall in spring and summer (Valeo et al, 2007; Pomeroy et al. 2010; 2014), but rainfall can be more important to streamflow generation in steeper mountain basins. Moreover, the connectivity of the wetland complex to basin outlet is important to streamflow generation in the Prairies and connectivity can be strongly regulated by ET which is enhanced by warming.

To reduce the computational effort and conduct hydrological modeling forced by 35 climate input scenarios in all the seven basin types, one representative AHCCD station was selected as an exemplar for each of the basin types. This is one of the limitations in this study, as the hydrological sensitivities associated with different baseline climates were not compared for the same basin class. Spence et al. (2022a) indicated that sensitivity to climate perturbation varied with local climate within the same Prairie basin class. The elasticity modeling here also demonstrated dynamic percentage changes in peak SWE with warming and per % P increase under different P and T input scenarios (Figure 5). Mean TES and PES used in this study were calculated as the average change rate in hydrological variables forced by the 35 climate inputs at the representative AHCCD stations, which are therefore reasonably used as the hydrological sensitivity assessment for the typical locations in each of the classes. In Spence et al. (2022a), simulating streamflow in HEG with a Medicine Hat climate resulted in an absolute TES 3.3 % °C⁻¹ higher than with a Brandon climate. In this study, when forcing the HEG VB model at Medicine Hat and the MRV VB model at Brandon, the TES difference for annual streamflow is as small as 1.0 % °C⁻¹ (Table 6). This suggests simulating streamflow in one basin class with a representative climate likely reduces uncertainty in the sensitivity assessment than running a VB model with a distant unrepresentative meteorology.



430 *TES* and *PES* showed distinct gradients from drier to wetter climates over the Prairies as the lower baseline SWE or annual
streamflow in the drier and grassland-characterized classes (Borchert, 1950; Millett et al. 2009; Pomeroy et al. 2010) likely
resulted in higher percentage change of response variables assessed herein (Eqs. 1–2). Whitfield et al. (2020) analyzed the
changing trends in the Prairies streamflow during 1920–2015 and demonstrated that streams in the southwestern Canadian
Prairies are shifting to drier conditions, and that the northeast is getting wetter. The modeling results here align with their
435 findings and partly reveal the underlying mechanisms: streamflow in the western HEG class and southern SI class declined
more rapidly with warming but increased more slowly with *P* rising than those in the eastern SM class and the northern MRV
class. Meanwhile, streamflow reduction in the eastern basins due to warming is more easily offset by *P* increase than in the
western basins. Forced by future warming, streamflow in the drier and grassland-characterized basins will probably continue
to get drier, and wetter cropland-dominated basins will continue to get wetter.

440 In addition to the climate difference, landscape traits among the basins also contributed to the varied hydrological sensitiv-
ities. For example, the SM class was characterized by fewer wetlands and higher connectivity than the other classes, which
resulted in smaller streamflow sensitivity to warming. The non-effective fraction in IG was much larger than that in SI, and
when forced by the same meteorological observations at Swift Current, streamflow in IG showed much larger sensitivities to
T and *P* perturbations. Wetland fraction and depressional storage capacity in PHT is larger than that in MRV. When forced by
445 similar climate at Yorkton and Brandon, streamflow, ET and CA in PHT showed larger sensitivities. This can be explained by
hydrological connectivity and streamflow generation in the PHT basins being more limited by water availability because of the
larger depressional storage capacity. However, the influence of landscape traits on sensitivity of basin-average snow to climate
perturbations was smaller than the influence of site climate.

High uncertainty in modeled sensitivities in the Prairies has been documented before (Unduche et al., 2018). Sources of
450 uncertainty in this study include those with VB model parameter estimation, inaccurate meteorological data from the AHCCD
station and the perturbed climate scenarios. The 35 perturbed climate scenarios were set up based on a delta approach with
the assumption that *P* and *T* perturb linearly without considering the seasonal dynamics. Despite that, the delta approach
facilitates the investigation of climate sensitivity based on a long-term simulation and has been acceptably used to represent
the uncertainty in the projected future climate over the Prairies (Zhang et al. 2021). The maximum warming of 6 °C, and the
455 future change range in *P* of -20% to +30% were derived from Canada's Changing Climate report edited by Bush and Lemmen
(2019) and projections by Jiang et al. (2017), and are close to the delta changes downscaled from a couple of GCMs in Forbes
et al. (2011). However, caution should be taken when extrapolating or interpolating these results to the specific basins, as
the modeling used VBs that represent the typical hydrological characteristics of a basin type in a hydroclimatic region of the
Canadian Prairies. The results are meant to reflect a regional response, rather than that in any specific location. Finally, using
460 the delta method does not allow for an assessment of hydrological sensitivity to specific or ensemble projections of climate
changes in the region.



5.2 Implications for adaptive water management strategies

Considering the freshwater availability risk caused by economic and population growth and agricultural expansion in the Prairies concomitant with climate change (St-Jacques et al., 2018), these scenario-based modeling results have important im-
465 plications for the development of adaptive strategies to changing climate for the Prairie Provinces. The sensitivity analysis based on a physically based hydrological model provides a diagnosis of the underlying processes behind hydrological response to climate change, and provides insightful information to support the design and direction of adaptive practices (Tarnoczi, 2011). Separation of P and T sensitivity could serve as guidance for adaptation strategies in response to short-term hydrologi-
470 cal flooding triggered by precipitation events, and long-term warming and droughts caused by decadal temperature increases (Zhang et al., 2021). Elasticity modeling of hydrological processes under variable climate and basin types over the Prairie provides useful information for how hydrological processes and streamflow may change and how the hydrological sensitivity to climate perturbations can differ, across the spectrum of climate and landscapes (Wheater and Gober, 2013). The sensitivity assessment indicated to what extent snow processes, soil moisture and streamflow will be significantly impacted by meteo-
475 rological forcing changes in the different regions, delivering informative knowledge for potential management of agricultural activities. The combined effects of P and T perturbations on soil moisture and streamflow have implications for the Prairie Provinces' climate change plans that are aimed at building climate resilience (Sauchyn et al., 2017), including improving understanding of future hydrology changes and the quantitative examinations of the tradeoff between P increase and warming, which importantly differ according to basin type and climate in the study region.

6 Conclusions

480 This study evaluated hydrological sensitivity to climate across the Canadian Prairies based on a basin-classification and virtual basin(VB) modeling approach, with different land covers represented with HRUs. Among the different land covers, snow accumulation in wetlands is more sensitive to climate perturbations than that in cropland and grassland. Peak SWE in cropland showed larger climate sensitivity than that in grassland in wet and cropland-dominated basin types (PGL, PHT, MRV and SM), but was less sensitive in the dry and grassland-characterized basin types (HEG, IG, and SI). Wetland soil moisture was more
485 sensitive to warming than that in cropland and grassland, with cropland soil moisture being the least sensitive to temperature (T). Precipitation (P) sensitivity for soil moisture in cropland, grassland and wetland tended to be consistent over the Prairies. Due to the joint influences of land cover and site climate, snow accumulation and melt runoff at the basin scale were more sensitive to warming in the drier and grassland-characterized basins than in the wetter and cropland-dominated basins. Basin-average soil moisture was more sensitive to T and P perturbations in basins typified by pothole depressions and broad river
490 valleys than that in grassland-characterized basins. Annual streamflow exhibited the greatest sensitivities to T and P in the dry and poorly connected IG basins but the smallest sensitivity to T in the wet and well-connected SM basins. The effectiveness of P increases in compensating for the effects of warming on snow accumulation and annual streamflow was higher in wet than in dry basins. For snow accumulation, the maximum 30% increase in P could fully offset warming of 3 °C in wet SM, but could only compensate for 2 °C in the dry and grassland-characterized basins (e.g. HEG). For annual streamflow, the maximum P



495 increase of 30% could offset decreases caused by warming of 6 °C in the wetter and cropland-dominated basins in the eastern prairies, but could not in the drier grassland-characterized basins of the western prairies.

These sensitivity analyses improved understanding of variations in hydrological responses to climate change over the Canadian Prairies, highlighting where important hydrological states for agricultural productivity (e.g. soil moisture) are sensitive and likely to change due to overwhelming effects of warming, even where potential P increases occur. Assessments of the sensitivities of snow processes, soil moisture, ET, and connected area provide diagnosis of the underlying processes behind streamflow response to climate change over the Prairies. Both basin characteristics and local climate played influences on the basin hydrological sensitivities. The lower P effectiveness in compensating for warming effects in the drier and grassland-characterized basins highlighted their tendency to undergo more drying than the wetter and cropland-dominated basins which are historically wetter. Interannual variability, particularly with anticipated new precipitation extremes, has not been considered here, and warrants further consideration. Adaptation strategies in the drier basins should be carefully designed for a future where surface water is scarcer. In the wetter basins concentrated in eastern parts of the study region, it seems the ability to cope with more water in many years will be necessary in the short term, but long-term drying is also possible.

Data availability. All climate forcing data, model output and parameter data will be publicly available via the Federated Research Data Repository.

510 *Author contributions.* CS, JWP and CJW conceived the study. ZH and KRS lead the modeling effort and data analysis. All authors contributed to writing.

Competing interests. The authors declare that they have no conflict of interest.

Acknowledgements. The authors wish to acknowledge funding provided by the Canada First Research Excellence Fund to the Global Water Futures that supported this research. Additional support from the Canada Research Chairs, and Natural Sciences and Engineering Research Council of Canada is gratefully acknowledged. The role of Mr. Tom Brown in developing and supporting the CRHM Platform in his 50-year hydrological modelling career at the University of Saskatchewan and the research findings of the Division of Hydrology and Centre for Hydrology at the same university were crucial to this research.



References

- Anteau, M.J., Wiltermuth, M.T., van der Burg, M.P., Pearse, A.T.: Prerequisites for Understanding Climate-Change Impacts on Northern
520 Prairie Wetlands, *Wetlands*, 36, 299–307, <https://doi.org/10.1007/s13157-016-0811-2>, 2016.
- Armstrong, R.N., Pomeroy, J.W., Martz, L.W.: Estimating evaporation in a Prairie landscape under drought conditions, *Canadian Water Resour. J.*, 35, 173–186, 2010.
- Armstrong, R.N., Pomeroy, J.W., Martz, L.W.: Variability in evaporation across the Canadian Prairie region during drought and non-drought periods, *J. Hydrol.*, 521, 182–195, <https://doi.org/10.1016/j.jhydrol.2014.11.070>, 2015.
- 525 Borchert, J. R.: The climate of the central north american grassland, *Ann. Assoc. Am. Geogr.*, 40, 1–39., <https://doi.org/10.1080/00045605009352020>, 1950.
- Bush, E. and Lemmen, D. S.: Canada's Changing Climate Report, Government of Canada, Ottawa, ON., <https://changingclimate.ca/CCCR2019>, 2019.
- Coles, A. E., McDonnell, J., McConkey, B. G.: Fifty Years of Recorded Hillslope Runoff on Seasonally Frozen Ground: The Swift Current,
530 Saskatchewan, Canada, Dataset, *Earth Syst. Sci. Data.*, 11 (3), 1375–83, <https://doi.org/10.5194/essd-11-1375-2019>, 2019.
- Cordeiro, M. R. C., Wilson, H. F., Vanrobaeys, J., Pomeroy, J. W. and Fang, X.: Simulating cold-region hydrology in an intensively drained agricultural watershed in Manitoba, Canada, using the Cold Regions Hydrological Model, *Hydrol. Earth Syst. Sci.*, 21(7), 3483–3506, doi:10.5194/hess-21-3483-2017, 2017.
- Cordeiro M. R. C.; Liang K.; Wilson H. F.; Vanrobaeys J.; Lobb D. A.; Fang, X.; Pomeroy, J. W., Simulating the hydrological impacts of land
535 use conversion from annual crop to perennial forage in the Canadian Prairies using the Cold Regions Hydrological Modelling platform., *Hydrol. Earth Syst. Sci.*, 26, (2022), 5917:5931, doi: 10.5194/hess-26-5917-2022, 2022.
- Costa, D., Shook, K., Spence, C., Elliott, J., Baulch, H., Wilson, H. and Pomeroy, J. W.: Predicting Variable Contributing Areas, Hydrological Connectivity, and Solute Transport Pathways for a Canadian Prairie Basin, *Water Resour. Res.*, 56(12), doi:10.1029/2020WR027984, 2020.
- 540 Fang, X. and Pomeroy, J. W.: Snowmelt runoff sensitivity analysis to drought on the Canadian prairies, *Hydrol. Process.*, 22(21), 2594–2609, doi:10.1002/hyp, 2007.
- Fang, X. and Pomeroy, J. W.: Modelling blowing snow redistribution to prairie wetlands, *Hydrol. Process.*, 23, 2557–2569, doi:10.1002/hyp.7348, 2009.
- Fang, X., Pomeroy, J. W., Westbrook, C. J., Guo, X., Minke, A. G. and Brown, T.: Prediction of snowmelt derived streamflow in a wetland
545 dominated prairie basin, *Hydrol. Earth Syst. Sci.*, 14(6), 991–1006, doi:10.5194/hess-14-991-2010, 2010.
- Forbes, K.A., Kienzle, S.W., Coburn, C.A., Byrne, J.M., Rasmussen, J.: Simulating the hydrological response to predicted climate change on a watershed in southern Alberta, Canada, *Clim. Change*, 105, 555–576, <https://doi.org/10.1007/s10584-010-9890-x>, 2011.
- Granger, R. J., Gray, D. M.: A net radiation model for calculating daily snowmelt in open environments, *Nordic Hydrology*, 21, 217 – 234, 1990.
- 550 Gray D. M.: Handbook on the Principles of Hydrology, Water Information Center, Inc. Port: Washington, NY, 1970.
- Gray, D.M., Toth, Brenda, Zhao, Litong, Pomeroy, J.W., Granger, R.J.: Estimating areal snowmelt infiltration into frozen soils, *Hydrol. Process.*, 15 (16), 3095–3111, 2001.
- Jiang, R., Gan, T. Y., Xie, J., Wang, N., Kuo, C.: Historical and potential changes of precipitation and temperature of Alberta subjected to climate change impact: 1900–2100, *Theor. Appl. Climatol.*, 127:725–739, 2017.



- 555 Johnson, W. C. and Poiani, K. A.: Climate Change Effects on Prairie Pothole Wetlands: Findings from a Twenty-five Year Numerical Modeling Project, *Wetlands*, 36, 273–285, doi:10.1007/s13157-016-0790-3, 2016.
- Johnson, W. C., Millett, B. V., Gilmanov, T., Voldseth, R. A., Guntenspergen, G. R. and Naugle, D. E.: Vulnerability of northern prairie wetlands to climate change, *Bioscience*, 55(10), 863–872, doi:10.1641/0006-3568(2005)055[0863:VONPWT]2.0.CO;2, 2005.
- Kienzle, S. W., Nemeth, M. W., Byrne, J. M. and MacDonald, R. J.: Simulating the hydrological impacts of climate change in the upper
560 North Saskatchewan River basin, Alberta, Canada, *J. Hydrol.*, 412–413, 76–89, doi:10.1016/j.jhydrol.2011.01.058, 2012.
- Leibowitz, S. G., Vining, K. C.: Temporal connectivity in a prairie pothole complex., *Wetlands*, 23(1), 13–25, 2003.
- MacDonald, R. J., Byrne, J. M., Boon, S. and Kienzle, S. W.: Modelling the Potential Impacts of Climate Change on Snowpack in the North Saskatchewan River Watershed, Alberta, *Water Resour. Manag.*, 26(11), 3053–3076, doi:10.1007/s11269-012-0016-2, 2012.
- Mahmood, T. H., Pomeroy, J. W., Wheeler, H. S. and Baulch, H. M.: Hydrological responses to climatic variability in a cold agricultural
565 region, *Hydrol. Process.*, 31(4), 854–870, doi:10.1002/hyp.11064, 2017.
- Mekis, É., L. A., Vincent: An overview of the second generation adjusted daily precipitation dataset for trend analysis in Canada, *Atmos.-Ocean*, 49, 163–177, 2011.
- Millett, B., Johnson, W.C., Guntenspergen, G.: Climate trends of the North American prairie pothole region 1906–2000, *Clim. Change*, 93, 243–267, <https://doi.org/10.1007/s10584-008-9543-5>, 2009.
- 570 Muhammad, A., Evenson, G. R., Stadnyk, T. A., Boluwade, A., Jha, S. K. and Coulibaly, P.: Impact of model structure on the accuracy of hydrological modeling of a Canadian Prairie watershed, *J. Hydrol. Reg. Stud.*, 21, 40–56, doi:10.1016/j.ejrh.2018.11.005, 2019.
- Pomeroy, J. W., Brown, T., Fang, X., Shook, K. R., Pradhananga, D., Armstrong, R., Harder, P., Marsh, C., Costa, D., Krogh, S. A., Aubry-Wake, C., Annand, H., Lawford, P., He, Z., Kompanizare, M., Lopez-Moreno, J. I.: The Cold Regions Hydrological Modelling Platform for hydrological diagnosis and prediction based on process understanding, *J. Hydrol.*, 615, 128711, <https://doi.org/10.1016/j.jhydrol.2022.128711>, 2022.
- 575 Pomeroy, J. W., Fang, X., Westbrook, C., Minke, A., Guo, X., Brown, T.: Prairie Hydrological Model Study Final Report, Centre for Hydrology Report No. 7, University of Saskatchewan, Saskatoon, 113 pp., <https://research-groups.usask.ca/hydrology/publications/reports.php>, 2010.
- Pomeroy, J., Fang, X., Ellis, C.: Sensitivity of snowmelt hydrology in Marmot Creek, Alberta, to forest cover disturbance, *Hydrol. Process*, 26, 1891–1904, 2012.
- 580 Pomeroy, J. W., Fang, X., Shook, K., Whitfield, P. H.: Predicting in ungauged basins using physical principles obtained using the deductive, inductive, and abductive reasoning approach, in: Pomeroy, J.W., Spence, C., Whitfield, P.H. (Eds.), *Putting Prediction in Ungauged Basins into Practice*, Canadian Water Resources Association, pp. 41–62, 2013.
- Pomeroy, J. W., Gray, D. M., Brown, T., Hedstrom, N. R., Quinton, W., Granger, R. J., Carey, S.: The cold regions hydrological model: a platform for basing process representation and model structure on physical evidence, *Hydrol. Process.*, 21, 2650–2667, 2007.
- 585 Pomeroy, J. W., Gray, D. M., Shook, K. R., Toth, B., Essery, R. L. H., Pietroniro, A., Hedstrom, N.: An evaluation of snow accumulation and ablation processes for land surface modelling, *Hydrol. Process.*, 12, 2339–2367, 1998.
- Pomeroy, J. W., Gray, D. M., Landine, P. G.: The Prairie Blowing Snow Model: characteristics, validation, operation, *J. Hydrol.*, 144, 165–192, 1993.
- 590 Pomeroy, J. W., Shook, K., Fang, X., Dumanski, S., Westbrook, C., Brown, T.: Improving and testing the prairie hydrological model at Smith Creek Research Basin, Centre for Hydrology Report No.14. May, 2014.



- Rasouli, K., Pomeroy, J. W., Whitfield, P. H.: Hydrological Responses of Headwater Basins to Monthly Perturbed Climate in the North American Cordillera., *J. Hydrometeorol.*, 20, pp.863:882, doi: 10.1175/JHM-D-18-0166.1, 2019.
- Rasouli, K., Pomeroy, J. W., Whitfield, P. H.: The sensitivity of snow hydrology to changes in air temperature and precipitation in three North American headwater basins., *J. Hydrol.*, 606, 127460, doi: 10.1016/j.jhydrol.2022.127460, 2022.
- 595 Samuel, J., Coulibaly, P., Kollat, J.: CRDEMO: Combined regionalization and dual entropy-multiobjective optimization for hydrometric network design, *Water Resour. Res.*, 49, 8070–8089, <https://doi.org/10.1002/2013WR014058>, 2013.
- Sauchyn, D., Davidson, D. and Johnston, M.: Prairie Provinces; Chapter 4 in *Canada in a Changing Climate: Regional Perspectives Report*, 2017.
- 600 Schaake, J. C.: From climate to flow. In: Waggoner, P.E. (Ed.), *Climate change and U.S. water resources*, 177–206, John Wiley and Sons Inc., New York, USA, 1990.
- Shahabul Alam, M. and Elshorbagy, A.: Quantification of the climate change-induced variations in Intensity-Duration-Frequency curves in the Canadian Prairies, *J. Hydrol.*, 527, 990–1005, doi:10.1016/j.jhydrol.2015.05.059, 2015.
- Shaw, D. A., Vanderkamp, G., Conly, F. M., Pietroniro, A., and Martz, L.: The Fill-Spill Hydrology of Prairie Wetland Complexes during Drought and Deluge, *Hydrol. Process.*, 26, 3147–3156, <https://doi.org/10.1002/hyp.8390>, 2012.
- 605 Shook, K., Pomeroy, J. W., Spence, C., and Boychuk, L.: Storage dynamics simulations in prairie wetland hydrology models: Evaluation and parameterization, *Hydrol. Process.*, 27(13), 1875–1889, doi:10.1002/hyp.9867, 2013.
- Shook, K., Pomeroy, J., and van der Kamp, G.: The transformation of frequency distributions of winter precipitation to spring streamflow probabilities in cold regions; case studies from the Canadian Prairies, *J. Hydrol.*, 521, 395–409, doi:10.1016/j.jhydrol.2014.12.014, 2015.
- 610 Spence, C., He, Z., Shook, K., Mekonnen, B., Pomeroy, J., Whitfield, C., and Wolfe, J.: Assessing hydrological sensitivity of grassland basins in the Canadian Prairies to climate using a basin classification–based virtual modelling approach, *Hydrol. Earth Syst. Sci.*, 26, 1801-1819, <https://doi.org/10.5194/hess-26-1801-2022>, 2022a.
- Spence, C., He, Z., Shook, K., Pomeroy, J., Whitfield, C., and Wolfe, J.: Assessing runoff sensitivity of North American Prairie Pothole Region basins to wetland drainage using a basin classification-based virtual modelling approach, *Hydrol. Earth Syst. Sci.*, 26, 5555–5575, <https://doi.org/10.5194/hess-26-5555-2022>, 2022b.
- 615 St-Jacques, J. M., Andreichuk, Y., Sauchyn, D. J., and Barrow, E.: Projecting Canadian Prairie Runoff for 2041–2070 with North American Regional Climate Change Assessment Program (NARCCAP) Data, *J. Am. Water Resour. Assoc.*, 54(3), 660–675, doi:10.1111/1752-1688.12642, 2018.
- Tanzeeba, S. and Gan, T. Y.: Potential impact of climate change on the water availability of South Saskatchewan River Basin, *Clim. Change*, 112(2), 355–386, doi:10.1007/s10584-011-0221-7, 2012.
- 620 Tarnoczi, T.: Transformative learning and adaptation to climate change in the Canadian Prairie agro-ecosystem, *Mitig. Adapt. Strateg. Glob. Chang.*, 16(4), 387–406, doi:10.1007/s11027-010-9265-7, 2011
- Unduche, F., Tolossa, H., Senbeta, D., and Zhu, E.: Evaluation of four hydrological models for operational flood forecasting in a Canadian Prairie watershed, *Hydrol. Sci. J.*, 63(8), 1133–1149, doi:10.1080/02626667.2018.1474219, 2018.
- 625 Wheeler, H. and Gober, P.: Water security in the Canadian Prairies: Science and management challenges, *Philos. Trans. R. Soc. A Math. Phys. Eng. Sci.*, 371(2002), doi:10.1098/rsta.2012.0409, 2013.
- Whitfield, P. H., Shook, K. R., and Pomeroy, J. W.: Spatial patterns of temporal changes in Canadian Prairie streamflow using an alternative trend assessment approach, *J. Hydrol.*, 582(December 2019), doi:10.1016/j.jhydrol.2020.124541, 2020.



- 630 Withey, P. and van Kooten, G. C.: The effect of climate change on optimal wetlands and waterfowl management in Western Canada, *Ecol. Econ.*, 70(4), 798–805, doi:10.1016/j.ecolecon.2010.11.019, 2011.
- Wolfe, J. D., Shook, K. R., Spence, C., and Whitfield, C. J.: A watershed classification approach that looks beyond hydrology: Application to a semi-arid, agricultural region in Canada, *Hydrol. Earth Syst. Sci.*, 23(9), 3945–3967, doi:10.5194/hess-23-3945-2019, 2019.
- Van Hoy, D. F., Mahmood, T. H., Todhunter, P. E., and Jeannotte, T. L.: Mechanisms of Cold Region Hydrologic Change to Recent Wetting in a Northern Glaciated Landscape, *Water Resour. Res.*, 56, 1–28, <https://doi.org/10.1029/2019WR026932>, 2020.
- 635 Valeo, C., Xiang, Z., Bouchart, F. J.-C., Yeung, P., and Ryan, M. C.: Climate Change Impacts in the Elbow River Watershed, *Canadian Water Resources Journal*, 32:4, 285–302, DOI: 10.4296/cwrj3204285, 2007.
- Zhang, H., Huang, G. H., Wang, D., and Zhang, X.: Uncertainty assessment of climate change impacts on the hydrology of small prairie wetlands, *J. Hydrol.*, 396(1–2), 94–103, doi:10.1016/j.jhydrol.2010.10.037, 2011.
- Zhang, Z., Bortolotti, L. E., Li, Z., Armstrong, L. M., Bell, T. W., and Li, Y.: Heterogeneous Changes to Wetlands in the Canadian Prairies
640 Under Future Climate, *Water Resour. Res.*, 57(7), 1–16, doi:10.1029/2020WR028727, 2021.